

Toward Efficient and Stable Perovskite Solar Cells: Choosing Appropriate Passivator to Specific Defects

Xin Zhou, Wenjing Qi, Jiale Li, Jian Cheng, Yameng Li, Jingshan Luo, Min Jae Ko, Yuelong Li,* Ying Zhao, and Xiaodan Zhang

With a certificated record efficiency of 25.2%, organometal halide perovskite (OHP) solar cells have experienced unprecedentedly rapid development in the past decade due to their extraordinary photoelectronic properties. However, because of the rapid processing conditions and complex precursor compositions, there are a large number of defects in polycrystalline OHP films, including point defects and 2D defects along grain boundary and on the surface. Unfortunately, these defects serve as the nonradiative recombination centers and exert negative effects on the degradation and performance of OHP layers, heavily limiting their further application for efficient photovoltaic devices. Herein, the formation origin of various defects as well as their detrimental effects on the efficiency and stability of perovskite solar cells (PSCs) are discussed, and recent passivation strategies for specific defects to minimize defect state density in the perovskite films are summarized. Finally, a brief outlook on the development trend of future passivation engineering is provided for deeper understanding of efficient and stable PSCs.

1. Introduction

Organometal halide perovskites (OHPs) have garnered widespread attention due to their remarkable photoelectronic characteristics: superior light absorption coefficient,^[1] tunable composition and bandgap,^[2,3] small exciton binding energy,^[4] and long carrier diffusion length.^[5] The power conversion efficiency (PCE) for single-junction perovskite solar cells (PSCs) has been boosted in recent years to reach a certified PCE of 25.2%,^[6] as Miyasaka and coworkers first used perovskite materials as the photosensitizer in dye-sensitized solar cells (DSSCs).^[7] Especially, after the invention of the first solid-state PSCs coupling with the solid-state Spiro-OMeTAD by Park and coworkers,^[8] the prominent progress has been stridden over the

past decade by vigorously manipulating the solvents,^[9,10] compositions,^[11,12] and interfacial modifications.^[13,14] The impressive efficiency not only benefits from the superior properties of perovskite, but also benefits from the affordable material cost and simple processability. All these credits have made PSCs a promising competitor for the next-generation photovoltaic technology.

In addition to efficiency, stability is another critical issue hindering the commercialization of PSCs.^[15,16] Several external stresses, such as moisture, light, oxygen, electric field, and heat, have been believed to affect the stability of PSCs, which cause the degradation of perovskite absorbers into various products, such as lead iodide (PbI_2), CH_3NH_2 , and iodine (I_2),^[17-19] and the resulting nonstoichiometric atomic ratios may lead to many types of defects. It has been reported that

a large density of charge traps existed at the interfaces and interior of polycrystalline perovskite films.^[20] In the light of previous reports, there are several major types of defects in perovskite materials that are harmful to solar energy conversion: 1) intrinsic 0D defects (point defects),^[21-23] 2) 2D defects, such as grain boundaries and surface defects,^[24,25] 3) impurities, like doping.^[26,27] The above defects indeed impede the further development of PSCs by influencing the perovskite crystallization kinetics, the carrier recombination process, the energy band alignment, and the phase structural stability.^[28]

The defects in perovskite films exert a dominating influence on the photovoltaic parameters of PSCs including the open-circuit voltage (V_{oc}), short-circuit current density (J_{sc}), and fill factor (FF).^[29-31] When PSCs are under operation, the electrons

X. Zhou, W. Qi, J. Li, J. Cheng, Prof. J. Luo, Prof. Y. Li, Prof. Y. Zhao, Prof. X. Zhang

Institute of Photoelectronic Thin Film Devices and Technology of Nankai University

Key Laboratory of Photoelectronic Thin Film Devices and Technology of Tianjin

Solar Energy Research Center of Nankai University
#38 Tongyan Road, Jinnan District, Tianjin 300350, P. R. China
E-mail: lyl@nankai.edu.cn

X. Zhou, W. Qi, J. Li, J. Cheng, Prof. J. Luo, Prof. Y. Li, Prof. Y. Zhao, Prof. X. Zhang

Collaborative Innovation Center of Chemical Science and Engineering
Renewable Energy Conversion and Storage Center of Nankai University
#94 Weijin Road, Nankai District, Tianjin 300072, P. R. China

Y. Li
College of Chemical and Pharmaceutical Engineering
Hebei University of Science and Technology
#26 Yuxiang Street, Yuhua District, Shijiazhuang 050018, P. R. China

Prof. M. J. Ko
Department of Chemical Engineering
Hanyang University
222 Wangsimni-ro, Seongdong-gu, Seoul 04763, Korea

 The ORCID identification number(s) for the author(s) of this article can be found under <https://doi.org/10.1002/solr.202000308>.

are excited into the conduction band under light illumination, tearing the internal quasi-Fermi levels in the perovskite layer, which is the origin of the V_{oc} .^[32] However, free carriers can be trapped by defects for nonradiative recombination, reducing the charge density and ultimately inducing a decrease in V_{oc} .^[33,34] Furthermore, the recombination and poor contact between different functional layers impede charge extraction efficiency, resulting in the reduction of J_{sc} and FF.^[35] According to Equation (1)^[32]

$$V_{OC} = V_{OC,rad} + \frac{K_B T}{q} \ln(\eta_{ext}) \quad (1)$$

where $V_{OC,rad}$ is the radiative limit of the open-circuit voltage, η_{ext} is the external luminescence quantum efficiency, q is the elemental charge, K_B is the Boltzmann constant, and T is temperature. To attain higher PCE of PSCs, it is essential to approach the radiative limit via inhibition of recombination losses. In addition, the modulation of perovskite film morphology for reducing pinholes and improving uniformity and roughness and the optimization of interface contact at perovskite/charge transport layers interface may also increase the J_{sc} and FF. Therefore, diverse types of defects should be ultimately eliminated or at least partially lessened for less nonradiative recombination and/or improved charge carrier transportation and collection and thus enhanced performance of PSCs. Most recently, defect passivation as a practical approach to suppress the charge recombination dynamics and heighten the performance of PSCs has been widely demonstrated, as shown by the remarkably increasing number of publications in Figure 1a.^[36–38] Shao et al. first introduced the concept of passivation by depositing the fullerene on the surface of perovskite absorbers to eliminate hysteresis for inverted planar PSCs.^[39] Since then, increasing numbers of new passivation molecules, for instance, salts,^[40,41] polymers,^[42–44] and organic or inorganic molecules,^[45,46] have been applied to reduce the defects by the strong interaction between perovskite and passivation molecules, as shown in Figure 1b, suppressing

the influence of the external stresses, and advancing the photovoltaic performance of PSCs.

In this Review, we elucidate the origin of various defects and ion migration on the perovskite surface and grain boundaries as well as their detrimental effects on the performance of PSCs, especially on the PCE and stability. We then summarize the recent passivation strategies for a specific type of defect to minimize defect density in the perovskite films. Based on the successful examples of passivation, the passivation mechanism has been thoroughly and deliberately discussed in this Review as we believe that rationally selecting appropriate passivation to specific defects will effectively promote the performance of PSCs. Finally, we describe a brief outlook on the future development trend of passivation engineering.

2. Various Types of Defects

As the solution-processed halide perovskite is a mixed ionic-electronic conductor,^[37,47] abundant defects are generated on the perovskite film surfaces and along grain boundaries.^[29,35,48] Particularly, point defects are easily formed in perovskite materials, as shown in Figure 2a–i, due to the low thermal stability and formation energies in Figure 2j–k.^[23,49–52] Considering methylammonium lead triiodide ($\text{CH}_3\text{NH}_3\text{PbI}_3$ or MAPbI_3 , where MA is methylammonium) perovskite as an example, intrinsic point defects contain vacancies (V_{MA} , V_{Pb} , and V_I), interstitials (MA_i , Pb_i , and I_i), and antisite substitutions (MA_{Pb} , MA_I , Pb_{MA} , I_{MA} , and I_{Pb}).^[21,53] In general, vacancy defects diffuse into perovskite crystallites and generate shallow electronic traps near band edges, whereas some interstitials and antisites are deep-level defects inside the bandgap.^[54–57] These defects induce interfacial charge recombination and have detrimental impacts on carrier dynamics and photocurrent hysteresis of PSCs.^[58,59] Therefore, reducing the number of defects via effective passivation strategies is critical to enhancing the efficiency and stability of PSCs. The passivation strategies and mechanisms of different defects are shown in Table 1.

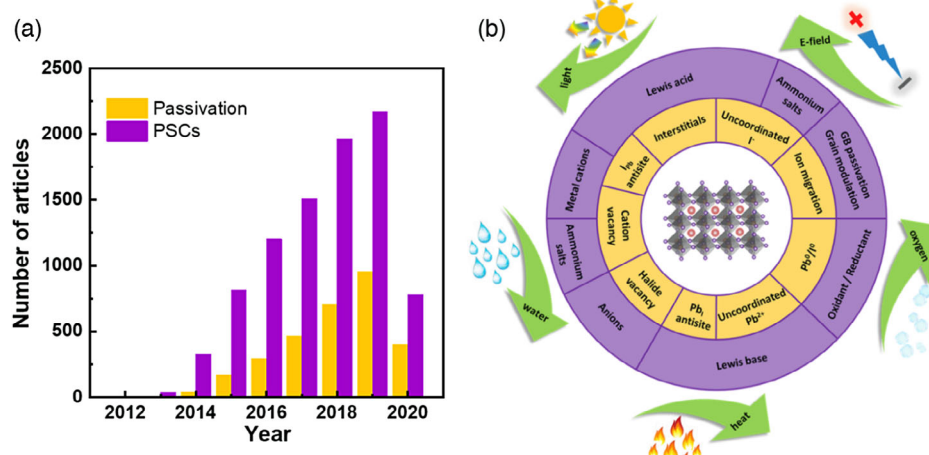


Figure 1. a) Number of articles on PSCs and passivation strategies (Updated by May 30, 2020); b) The types of defects in OHP films and their corresponding passivation strategies to prevent the decomposition from the external stimuli such as UV light, water, heat, oxygen, electric field, and so on.

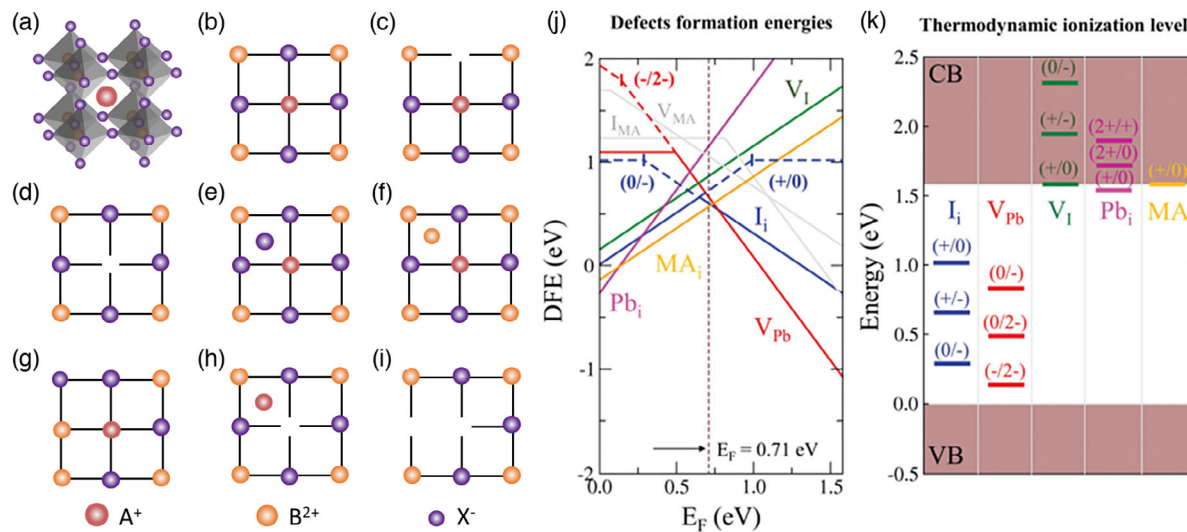


Figure 2. a) Perovskite crystal structure. (A^+ = monovalent cation; B^{2+} = metal cation; X^- = halide anion). Schematic illustration of point defects in perovskite crystal lattice: b) perfect lattice; c) halide vacancy; d) A-site ion vacancy; e) halide interstitial; f) metal ion interstitial; g) antisite substitution; h) Frenkel defect; i) Schottky defect. j) Defect formation energy (DFE, eV) diagram versus the Fermi energy (E_F , eV) for MAPbI_3 grown in stoichiometric conditions. k) Thermodynamic ionization levels for the most stable defects calculated in j). Reproduced with permission.^[49] Copyright 2018, Royal Society of Chemistry.

2.1. Vacancies

Under the thermal annealing conditions, the organic components MA or FA (where FA is formamidinium) and the volatile components like I_2 are prone to evaporate from the perovskite surface, accelerating the formation of organic cation vacancies and halide vacancies.^[108–111] In addition, Steirer et al. observed that the MAPbI_3 films continuously exposed to X-ray irradiation lost MA and I and subsequently formed V_{MA} and V_{I} .^[22] This is similar to the conclusion of Mosconi's study.^[112] They indicated that I vacancy/interstitial defect pairs were annihilated under light induction, resulting from the low migration energy of I defects. In addition, local lattice strain can also facilitate vacancy defects formation.^[60] Saidaminov et al. proposed that incorporating small cadmium (Cd) ions equivalent to Pb into perovskite lattice could relax the lattice strain and further suppress vacancies. What's more, vacancy-assisted ion migration aggravates the chemical decomposition of perovskite and deteriorates the stability of perovskite devices.^[113,114] As shown by Aristidou's study,^[113] I vacancies are occupied for forming superoxide species from oxygen (O_2) in the films exposed to light, leading to the degradation reaction. Thus, it is considered that passivation of ion vacancies is a highly key way to further optimize device performance.

2.1.1. Cation Vacancy

To effectively suppress the formation of cation vacancies, one method is to add excess MA/FA into the precursor solution or on the surface of perovskite film to compensate for their loss during the thermal annealing process.^[61] As shown in Figure 3a-d, Yang et al. demonstrated that the MAPbI_3 film with post-treatment of methylammonium bromine (MABr) turned

into quality-improved $\text{MAPbI}_{3-x}\text{Br}_x$ films with pinhole-free, large-grain, and high crystallinity via an Ostwald ripening process. Son et al. also reported that incorporating additional MAI into precursor solution generated a self-formed MAI layer on perovskite grains, which is beneficial to reduce carrier recombination losses and maximize charge extraction on the interface.^[62] Recently, Kim et al. realized an outstanding efficiency of 23.48% in FAPbI₃-based PSCs via methylammonium chlorine (MACl) addition.^[63] They revealed that the MACl contributes to stabilizing the α -phase FAPbI₃ perovskite structure only by the substitution of the cationic site and significantly improves the film quality. Another approach to hinder the generation of cation vacancies is to use larger organic molecules that are not easy to evaporate for building a low-dimensional (LD) layer structure. As early as 2016,^[64] Wang et al. discovered that utilizing a benzylamine molecule with a benzene ring and amine group to modify perovskite surface can prevent the penetration of water molecules into the perovskite absorber and elevate the formation energy of surface vacancy. Considering the superior environmental stability of 2D perovskite, it is a feasible way to introduce 2D perovskite into 3D perovskite to maintain the ambient stability while ensuring the high-level performance of PSCs.^[65,115] Niu et al. demonstrated that 2D Ruddlesden-Popper (RP) perovskite played a vital role in crystallization kinetics of the RP/3D heterostructure film in Figure 3e,f.^[115] Liu et al. recently reported that pentafluoro-phenylethylammonium (FEA) could replace organic cation or occupy organic cation vacancy to absorb on the 3D perovskite surface, and its 2D perovskite (FEA)₂PbI₄ deposited on the top of 3D perovskite layer could effectively keep moisture away from the film surface while mitigating ion migration.^[65] Remarkably, the efficiency of this 3D/2D bilayer-based PSCs exceeds 22% due to significant improvement in V_{oc} . Kim et al. compared the effects of

Table 1. Summary of the passivation strategies of various defects.

Passivator	Structure	Peroxskite components	Passivation functional groups	Target defect	Passivation mechanism	V _{oc} [V] (C/P ^a)	PCE [%] (C/P ^a)	Ref.	
BAI		(FAPbI ₃) _{0.95} (MAPbBr ₃) _{0.05}	BA ⁺	Ion vacancy	Electron blocking	1.09/1.11	21.23/21.71	[14]	
OAI		(FAPbI ₃) _{0.95} (MAPbBr ₃) _{0.05}	OA ⁺	Ion vacancy	Electron blocking	1.09/1.12	21.23/22.03	[14]	
DAI		(FAPbI ₃) _{0.95} (MAPbBr ₃) _{0.05}	DA ⁺	Ion vacancy	Electron blocking	1.09/1.13	21.23/21.89	[14]	
EAI		FA _{0.9} Cs _{0.07} MA _{0.03} Pb(I _{0.92} Br _{0.08}) ₃	EA ⁺ , I ⁻	Ion vacancy	Vacancy filling	1.07/1.12	20.72/22.3	[40]	
IAI		FA _{0.9} Cs _{0.07} MA _{0.03} Pb(I _{0.92} Br _{0.08}) ₃	IA ⁺ , I ⁻	Ion vacancy	Vacancy filling	1.07/1.10	20.72/21.6	[40]	
Gual		FA _{0.9} Cs _{0.07} MA _{0.03} Pb(I _{0.92} Br _{0.08}) ₃	Gua ⁺ , I ⁻	Ion vacancy	Vacancy filling	1.07/1.10	20.72/20.9	[40]	
PEAI		FA _{0.92} MA _{0.08} PbI ₃	PEA ⁺ , I ⁻	I ⁻ vacancy	Vacancy filling	1.12/1.16	21.2/23.5	[41]	
CdI ₂		Cd ²⁺	Halide vacancy		Strain relaxation	1.160/1.164	20.8/21.0	[60]	
MABr		MA ⁺ , Br ⁻	Ion vacancy		Grain modulation	1.08/1.12	16.63/19.12	[61]	
MAI		MA ⁺ , I ⁻	Ion vacancy		Vacancy filling	-/1.17	-/20.4	[62]	
MACl		MA ⁺ , Cl ⁻	Ion vacancy		Phase Stabilization	1.03/1.13	19.66/24.02	[63]	
Benzylamine		FA0.92MA0.04Cs0.04PbI ₃	-NH ₂	I ⁻ vacancy	Hydrogen bonding	1.01/1.12	15.7/19.2	[64]	
FEAI		FA _{0.92} MA _{0.04} Cs _{0.04} PbI ₃	FEA ⁺	Cationic vacancy	Vacancy filling	1.045/1.096	20.6/22.2	[65]	
NA ⁺		NA ⁺			MA vacancy	Vacancy filling	1.05/1.06	18.8/20.2	[66]
NaF		NaF	(Cs _{0.05} FA _{0.54} MA _{0.41})Pb(I _{0.98} Br _{0.02}) ₃	F ⁻	Ion vacancy	Hydrogen bonding Ionic bonding	1.095/1.126	19.68/21.92	[67]
DPSI		FA _{0.85} MA _{0.15} Pb _{2.55} Br _{0.4}	-N(CH ₃) ₃ ⁺ , -SO ₃ ⁻	I ⁻ vacancy	Vacancy filling	1.06/1.13	19.1/21.1	[68]	
KI		KI	(Cs _{0.06} FA _{0.7} MA _{0.15})Pb(I _{0.85} Br _{0.15}) ₃	K ⁺ , I ⁻	Halide vacancy	Vacancy filling/immobilizing	1.05/1.17	17.3/21.5	[69]
KCl		KCl	MAPb _{3-x} Cl _x	K ⁺ , Cl ⁻	Halide vacancy	Vacancy filling	1.108/1.124	18.12/19.44	[70]
CdI ₂		CdI ₂	Rb _{0.025} Cs _{0.025} FA _{0.70} MA _{0.25} PbI ₃	Cd ²⁺ , I ⁻	I ⁻ vacancy	Vacancy filling/immobilizing	1.16/1.20	20.2/21.9	[71]
MACl+I ⁻		CH ₃ NH ₃ Cl, I ⁻	CsFAMAPb(I _{3-x} Br _x) ₃	Cl ⁻ , I ⁻	Halide vacancy	Grain modulation	1.162/1.193	20.49/21.65	[72]
Choline Chloride		Cl ⁻	FA _{0.85} MA _{0.15} Pb(I _{0.85} Br _{0.15}) ₃	-N(CH ₃) ₃ ⁺ , Cl ⁻	Pb ₃ ⁻ antisite Pb clusters	Vacancy filling Ionic bonding	1.03/1.14	19.2/21.0	[37]

Table 1. Continued.

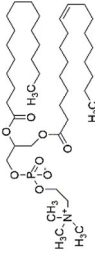
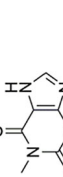
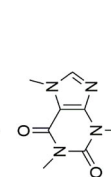
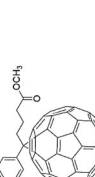
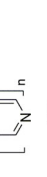
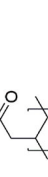
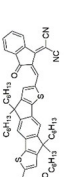
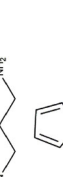
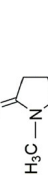
Passivator	Structure	Peroyskite components	Passivation functional groups	Target defect	Passivation mechanism	V_{oc} [V] (C/P^a)	PCE [%] (C/P^a)	Ref.	
L- α -phosphatidylcholine		MAPbI ₃	-N(CH ₃) ₃ ⁺ , -PO ₄ ⁻	PbI ₃ ⁻ antisite Pb clusters	Ionic bonding	1.04/1.08	17.1/19.6	[37]	
Theophylline		(FAPbI ₃) _x (MAPbBr ₃) _{1-x}	C=O N-H	Pb ₁ antisite	Coordinate bonding Hydrogen bonding	1.164/1.191	21.02/23.48	[73]	
Caffeine		(FAPbI ₃) _x (MAPbBr ₃) _{1-x}	C=O	Pb ₁ antisite	Coordinate bonding	1.164/1.178	21.02/22.32	[73]	
PCBM		MAPbI ₃		Fullerene	PbI ₃ ⁻ antisite	Coordinate bonding	1/1.086	8.6/14.4	[74]
NiCl ₂		MAPbI ₃	Ni ²⁺	PbI ₃ ⁻ antisite	Coordinate bonding	1.08/1.13	17.25/20.61	[75]	
KI		F _A _{0.85} M _A _{0.15} Pb _{1.255} Br _{0.45}	K ⁺	I interstitial	Occupying interstitial sites	1.122/1.131	17.83/17.85	[76]	
O ₂		MAPbI ₃	O ₂	I interstitial	Oxidation	—	—	[77]	
PAA		MAPbI ₃	-COOH	Uncoordinated Pb ²⁺	Coordinate bonding	1.09/1.16	18.05/19.65	[44]	
PVP		MAPbI ₃	Pyridine	Uncordinated Pb ²⁺	Coordinate bonding	1.09/1.15	18.05/20.23	[44]	
IDIC		MAPbI ₃	-C=O, -C≡N	Uncordinated Pb ²⁺	Coordinate bonding	1.03/1.11	13.5/19.5	[78]	
DAP		MAPbI ₃	Thiophene	Uncordinated Pb ²⁺	Coordinate bonding	1.08/1.18	18.3/21.7	[79]	
Thiophene		MAPb _{3-x} Cl _x	-NH ₂	Uncordinated Pb ²⁺	Coordinate bonding	0.95/1.02	13.1/15.3	[80]	
Pyridine		MAPb _{3-x} Cl _x	N donor	Uncordinated Pb ²⁺	Coordinate bonding	0.95/1.05	13.1/16.5	[80]	
NMP		FAPbI ₃	O donor	Uncordinated Pb ²⁺	Coordinate bonding	1.040/1.051	15.29/17.23	[81]	

Table 1. Continued.

Passivator	Structure	Perovskite components	Passivation functional groups	Target defect	Passivation mechanism	V_{OC} [V] (C/P^a)	PCE [%] (C/P^a)	Ref.
CH ₃ O-PEAI	H ₃ CO-phenyl-NH ₃ ⁺	(FAPbI ₃) _{1-x} (MAPbBr _{3-y} Cl _y) _x	Benzene ring	Uncoordinated Pb ²⁺	Electrostatic interaction	1.11/1.18	19.98/22.98 [82]	
Caffeine		MAPbI ₃	-CH ₃ O -C=O	Uncoordinated Pb ²⁺	Coordinate bonding	1.074/1.143	17.59/20.25 [83]	
Cl-CO		FA _x MA _{1-x} Pb _{1+y} I ₃	O donor, Cl ⁻	Uncoordinated Pb ²⁺	Coordinate bonding	1.09/1.12	20.00/21.08 [84]	
I-satin-Cl		MAPbI ₃	-C=O	Uncoordinated Pb ²⁺ MA vacancy	Coordinate bonding Hydrogen bonding	1.075/1.083	18.13/20.18 [85]	
Thiourea		MAPbI ₃	S donor -NH ₂	Uncoordinated Pb ²⁺	Coordinate bonding	0.881/0.910	10.20/13.03 [86]	
Thiourea		MAPbI ₃	S donor	Uncoordinated Pb ²⁺	Hydrogen bonding	1.03/1.09	16.6/19.8 [87]	
IT-M		C50.05(MA0.17FA0.83)0.95Pb(I0.83Br0.17)3	-C=O	Uncoordinated Pb ²⁺	Coordinate bonding	1.11/1.14	18.63/19.70 [88]	
SN		FA _{0.9} Cs _{0.1} PbI ₃	-SH, -NH ₃ ⁺	Uncoordinated Pb ²⁺ Cation vacancy	Coordinate bonding Ionic bonding	1.13/1.15	19.2/20.9 [89]	
DS		MAPbI ₃	S donor	Uncoordinated Pb ²⁺	Chelation	1.090/1.103	17.03/18.40 [90]	
N-RGO		FA _{0.85} MA _{0.15} Pb(I _{0.83} Br _{0.15}) ₃	O donor	Uncoordinated Pb ²⁺	Coordinate bonding Hydrogen bonding	1.12/1.15	17.3/18.7 [91]	
IPFB		MAPbI ₃	I substituent acceptor	Uncoordinated I ⁻	Halogen bonding	1.02/1.06	13.0/15.7 [92]	
2-aminoterephthalic acid		MAPbI ₃	-NH ₂ -COOH	Uncoordinated Pb ²⁺ Uncoordinated I ⁻	Coordinate bonding	1.08/1.12	19.13/21.09 [93]	

Table 1. Continued.

Passivator	Structure	Pero�skite components	Passivation functional groups	Target defect	Passivation mechanism	V _{oc} [V] (C/P) ^{a)}	PCE [%] (C/P) ^{a)}	Ref.
H ₄ Hc	HO—NH ₃	MAPbI ₃	—OH	Uncoordinated I [—]	Hydrogen bonding	1.05/1.10	16.85/18.69	[94]
CAI	NH ₂ H ₂ N—NH ₂ ⁺	MAPbI ₃	CA ⁺	Uncoordinated I [—]	Hydrogen bonding	1.025/1.071	16.35/17.13	[95]
Cu(Tu)I	Cu(H ₂ N—NH ₂) ₂ ⁺	MAPbI ₃	Cu ⁺ , I [—]	Uncoordinated I [—]	Chelation	1.00/1.12	11.1/19.9	[96]
HPA	H ₃ PO ₂	MAPbI ₃	PO ₂ ^{3—}	I [—] vacancy	Ionic bonding	1.07/1.07	13.2/16.2	[97]
Eu(acac) ₃	Eu ³⁺ —Eu ²⁺	MAPbI ₃	Pb ⁰ , I ⁰	I ₂	Reducing action	-/-1.15	-/-21.89	[98]
BQ		MAPbI ₃	O donor	Pb ⁰	Oxidation	1.02/1.02	10.73/15.56	[99]
ML	FA _{0.82} MA _{0.13} CS _{0.05} PbI _{2.87} Br _{0.13}		—SH	Uncoordinated Pb ²⁺	Coordinate bonding	1.07/1.16	19.0/21.4	[100]
D4TBP	Cs _{0.05} FA _{0.81} MA _{0.14} PbI _{2.55} Br _{0.45}		—NH ₂ , —COOH, benzene ring	I [—] vacancy	Ionic bonding	1.08/1.23	19.1/21.4	[101]
PCBA	FA _{0.75} MA _{0.25} PbI _{2.75} Br _{0.25}	C60	I ₂	Coordinate bonding	Strain relaxation	1.030/1.081	17.9/20.1	[102]
CsPbBr ₃	Cs _{0.05} FA _{0.80} MA _{0.15} Pb(I _{0.85} Br _{0.15}) ₃	CsPbBr ₃ -cluster	Ion migration	Core-shell structure	1.16/1.195	20.1/20.6	[103]	
BAI	FA _{0.83} CS _{0.17} Pb(I _{0.6} Br _{0.4}) ₃	BA ⁺	Phase segregation					
TiO ₂	MAPbI ₃	Ti ⁴⁺	Ion migration	Physical barrier	1.14/1.18	16.9/17.2	[104]	
PCBM	MAPbI ₃	Fullerene	Ion migration	Ionic bonding	1.068/1.084	16.7/17.42	[105]	
CsCl	MA _{0.03} FA _{0.97} Pb(I _{0.9} Br _{0.03}) ₃	Cs ⁺ , Cl [—]	Ion migration	Coordinate bonding	-/-	8/15.6	[106]	

^{a)}C/P represents the parameters of control/passivated device.

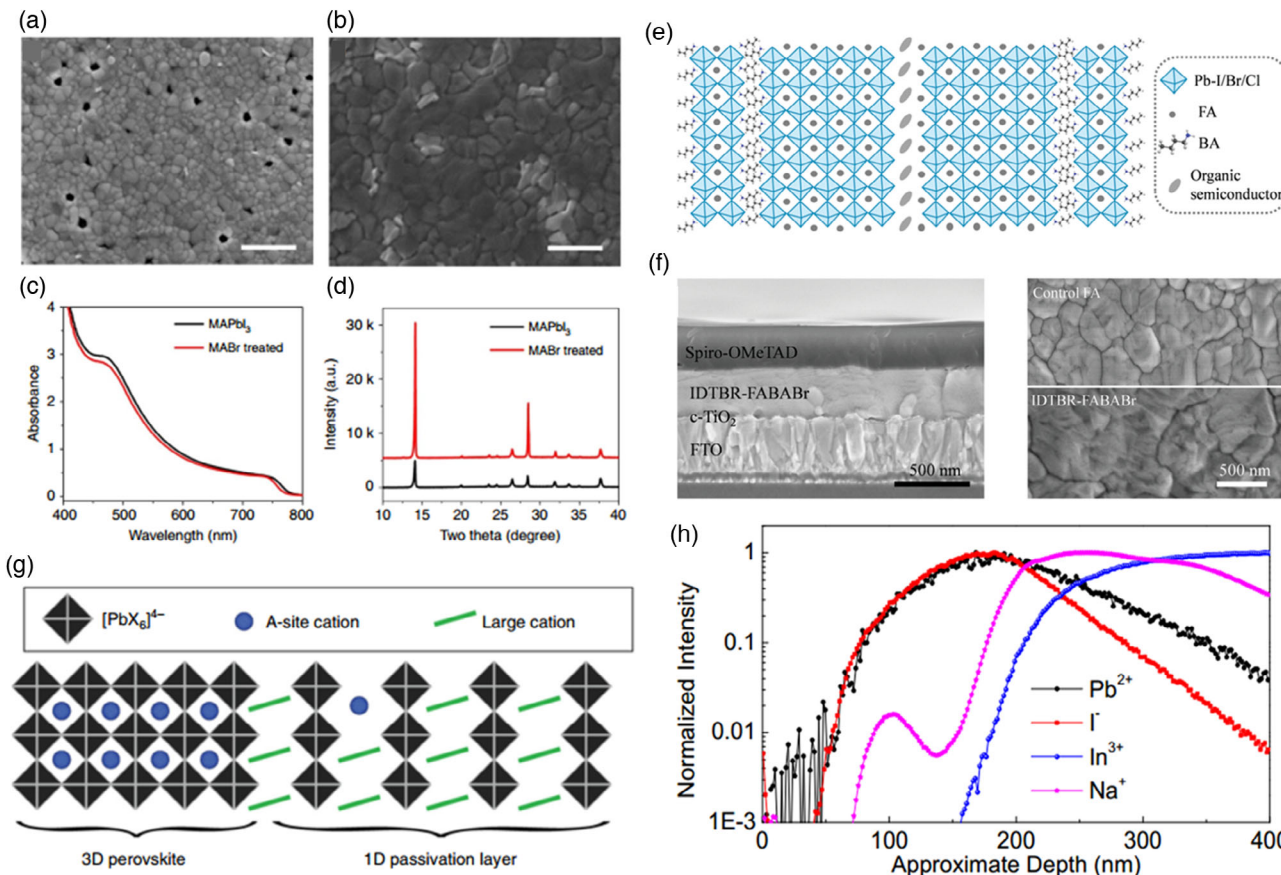


Figure 3. The impact of MABr treatment on the scanning electron microscopy (SEM) images of film morphology (MAPbI₃ films a) without and b) with MABr treatment, c) ultraviolet-visible (UV-vis) absorption spectra, and d) XRD patterns of the perovskite films. Reproduced with permission.^[61] Copyright 2016, Springer Nature. e) Schematic illustration and f) SEM images of the molecule-passivated RP/3D heterostructure. Reproduced with permission.^[115] Copyright 2018, Royal Society of Chemistry. g) Schematic representation of the 1D/3D heterostructure evidenced by solid-state NMR proximity measurements. Reproduced with permission.^[40] Copyright 2019, Springer Nature. h) Secondary-ion mass spectrometry (SIMS) measurement of interdiffusion-grown MAPbI₃ films on indium tin oxide (ITO) glass. Reproduced with permission.^[66] Copyright 2017, American Chemical Society.

alkylammonium iodide with different alkyl chain lengths, such as butylammonium (BA⁺), octylammonium (OA⁺), and dodecylammonium (DA⁺), for forming a 2D perovskite layer on the efficiency and moisture resistance of PSCs. As the alkyl chain length increasing, the electron-blocking properties and resistance against humidity of the 3D/2D PSCs were enhanced, whereas the OA⁺-treated PSC obtained an optimal PCE of 22.9%.^[14]

Moreover, 1D perovskite structures can also be formed by other organic molecules, including ethylammonium iodide (EAI),^[40] 1,1,1-trifluoro-ethyl ammonium iodide (FEAI),^[116] and imidazolium iodide (IAI).^[117] Alharbi et al. applied solid-state nuclear magnetic resonance (NMR) to confirm that EAI, IAI, and guanidinium iodide (GuaI) formed a 1D passivation layer on the perovskite grains in Figure 3g, which inhibited the interfacial nonradiative recombination through the formation of 3D/1D heterostructure with high ambient stability and passivation of iodide vacancies.^[40] Therefore, LD perovskite layer can not only significantly enhance humidity resistance, but also reduce the hysteresis by impeding the ion diffusion. In addition, metal ions have also been investigated for their promising passivation effect of organic cation vacancies.^[46,118] Bi et al. first reported that sodium ions (Na⁺) have the ability of passivating

grain boundaries.^[66] Partial Na⁺ from the substrates could diffuse into the film when the PSCs were stored for a period in nitrogen in Figure 3h. They proposed that Na⁺ could be adsorbed on MA⁺ vacancies to reduce defect density, thus improving the PCE of the device from 18.8% to 20.2%.

Alkylammonium salts as a kind of mainstream passivator have the ability to boost device performance and stability by doping into the surface or grain boundaries of the absorber layer or forming a layered perovskite phase. Excessive ammonium salts such as MA or FA as the raw components of perovskite materials are used to promote grain growth with improved crystallinity and surface morphology, which is a reasonably simple and efficient method for healing cation vacancies in the bulk and on the surface. Furthermore, some bulky ammonium salts with long carbon chain or large group that does not incorporate into the perovskite lattice can induce the formation of LD-layered structures. Although the layered perovskite may impair carrier transportation, the heterostructure formed with the 3D perovskite has a powerful synergistic passivation effect of defect elimination and nonradiative recombination reduction by establishing type-I band alignment as well as moisture resistance and suppression of ion migration by providing a physical block.

2.1.2. Halide Vacancy

With regard to halide vacancies, excess halide ions are introduced into the perovskite absorber layer for reducing the content of halogen vacancies. Some metal halides and ammonium halide salts have been reported to play an important role in filling or inhibiting halide vacancy formation through ionic bonding,^[67,68] hydrogen (H) bonding^[69,76] or lattice strain relaxation.^[60,119]

Abdi-Jalebi et al. indicated that potassium iodide (KI) incorporated into the precursor solution could compensate for the loss of halide ions, thereby suppressing the pathways of charge nonradiative recombination and vastly improving the luminescence efficiencies.^[69] Later, Wang et al. inserted a thin layer of potassium chloride (KCl) at $\text{SnO}_2/\text{MAPbI}_{3-x}\text{Cl}_x$ interface to boost device efficiency. The K^+ and Cl^- could diffuse into the absorber layer to fill ion vacancies and heal the grain boundaries during the annealing process of perovskite films, as shown that perovskite film absorbed the KCl grains in Figure 4a,b. The KCl-passivated method is conducive to the enhancement of perovskite crystallinity and light absorption capacity and the reduction of defect states.^[70] In addition, Huang et al. proposed a strategy for effective surface passivation of blade-coated perovskite films using cadmium iodide (CdI_2)-coating treatment shown in Figure 4c. Cd^{2+} can replace part of Pb^{2+} to inhibit the formation of halide vacancy due to the stronger Cd—I bond energy. At the same time, excess I^- provided by CdI_2 can fill the iodide vacancy on the surface. The CdI_2 -modified PSC achieved a high PCE of 21.9%, exhibiting a high V_{oc} up to 1.2 V with a

smallest V_{oc} loss of 0.31 V.^[71] Beyond metal halides, halide ions were also introduced in the form of ammonium halide. Tavakoli et al. utilized MACl to modulate perovskite crystallization for the purpose of optimizing the morphology of thin films with large grain. And the halide vacancies left on the perovskite surface were further passivated with iodine due to the volatilization of Cl during the annealing process.^[72] You et al. adopted phenethylammonium iodide (PEAI) to passivate the surface defects of FA-MA mixed perovskite films by post-processing at room temperature. From the X-ray diffraction (XRD) results, with the increase in annealing temperature, PEAI is gradually converted into the 2D PEA_2PbI_4 . It concluded that PEAI crystal itself without thermal annealing is superior in passivation effect compared with 2D PEA_2PbI_4 perovskite. The iodide ions from the PEAI can fill the halide vacancies on the perovskite film surface and $\pi-\pi$ bonding from the benzene ring reduces the neutral iodine-related defects, suppressing the recombination and improving the device performance. The certificated PCE of the best device is as high as 23.32%.^[41]

At present, the multivacancy defect passivation engineering has also been actively studied. In a recent study, Li et al. revealed that sodium fluoride (NaF) could play a critical role in simultaneously blocking the formation of organic cation and halide anion vacancies. F ions with high electronegativity assist the formation of hydrogen bonds with MA/FA ions and enhance the ionic bond with Pb^{2+} in the perovskite layer, which suppresses the diffusion and dissociation of the MA/FA ions and stabilizes the perovskite crystal structure in Figure 4d-g.

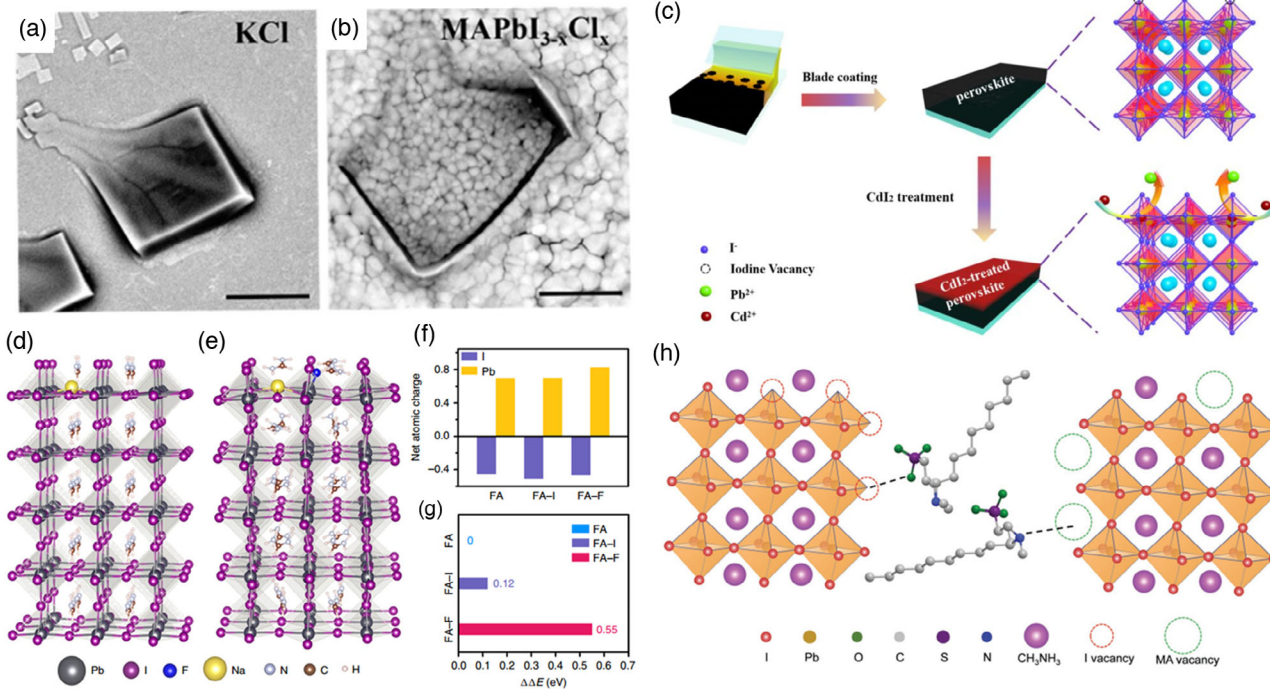


Figure 4. Top-SEM images of KCl film a) with high concentration and b) that coated perovskite film. Scale bars stand for 3 μm . Reproduced with permission.^[70] Copyright 2018, Royal Society of Chemistry. c) Schematic illustration of blade-coated perovskite film with CdI_2 surface treatment. Reproduced with permission.^[71] Copyright 2020, American Chemical Society. d,e) Location of Na and F ion in the FAPbI_3 . f) The change of ionic charge on I and Pb ions. g) The formation energy of a surface FA vacancy. Reproduced with permission.^[67] Copyright 2019, Springer Nature. h) Schematic illustration of DPSI-mediated perovskite defect passivation. Reproduced with permission.^[68] Copyright 2018, John Wiley and Sons.

As a result, a certified efficiency of 21.3% in the device was obtained, and the device maintained 90% of its original PCE after 1000 h of continuous 1-sun irradiation at the maximum power point (MPP).^[67] Later on, Huang and coworkers used a sulfonic zwitterion, 3-(decyldimethylammonio)-propane-sulfonate inner salt (DPSI) that includes a quaternary ammonium cationic group and a sulfonic group with negative charge, to tune the crystallization behavior and passivate defect states of perovskite films. As shown in Figure 4h, the S=O bond with lone pairs of electrons from the sulfonic group could bind to Pb²⁺ ions to form strong coordination bonds during the film processing, which controls the growth process of perovskite crystals and restrains the formation of pinhole. Then the DPSI molecules enabled their charged functional groups to fill defects with opposite charges on the film surfaces and at grain boundaries after the perovskite layer formation.^[68]

Control and reduction of the amount of cation and halide anion vacancies are essential to improve carrier transport dynamics. Although the current research on mitigating vacancy defect density has made great progress, most passivation methods can only suppress a single defect type, thus multivacancy defect passivation such as quaternary ammonium zwitterions needs to be developed to fully compensate for ion vacancies by a combination of hydrogen bonds and electrostatic interaction.

2.2. Pb-I Antisite Defects

Early studies proved that Pb-I antisite defects form deep-level traps,^[21] and are the dominant source of defects on the surface

of perovskite film.^[73,120] Pb-I antisite defects include Pb_I and I_{Pb} defects. Among them, Pb_I antisite means that Pb occupies the I site and belongs to donor defects, whereas I_{Pb} (PbI₃⁻) means that the Pb site is substituted by I and belongs to acceptor defects.^[29] Thus, Pb-I antisite defects can cause carrier nonradiative recombination during device operation, thereby affecting device performance. So far, several passivating agents have been used as electron donors or acceptors to interact with antisite deficiency and subsequently eliminate the related deep traps.^[37,73-75]

Xu et al. reported the perovskite-PCBM ([6,6]-phenyl-C61-butrylic acid methyl ester) hybrid films could effectively suppress hysteresis and enhance photovoltage for planar PSCs. When PCBM was added to the perovskite precursor solution, PCBM halide radicals are formed, which can be confirmed as a peak at 1020 nm in the absorption spectrum, as shown in Figure 5a.^[121] Practically, PCBM can be evenly distributed throughout the film layer, and combines with PbI₃⁻ antisite defect at the grain boundaries, inhibiting the formation of deep-level defect states.^[74] Zheng et al. firstly proved that choline zwitterions could passivate both negatively charged PbI₃⁻ antisite defects and positively charged Pb ion cluster, reaching a certified efficiency of 20.59% for PSCs. The energy band structure model and the density of states (DOS) of two typical defects surface passivated by choline halide molecules are shown in Figure 5b,c. The bond of Pb ion cluster with Cl⁻ and I⁻ formed new hybrid states that connect the defect state with the conduction band edge state of the surface, suppressing charge trapping. Meanwhile, the DOS results show that the gap states of

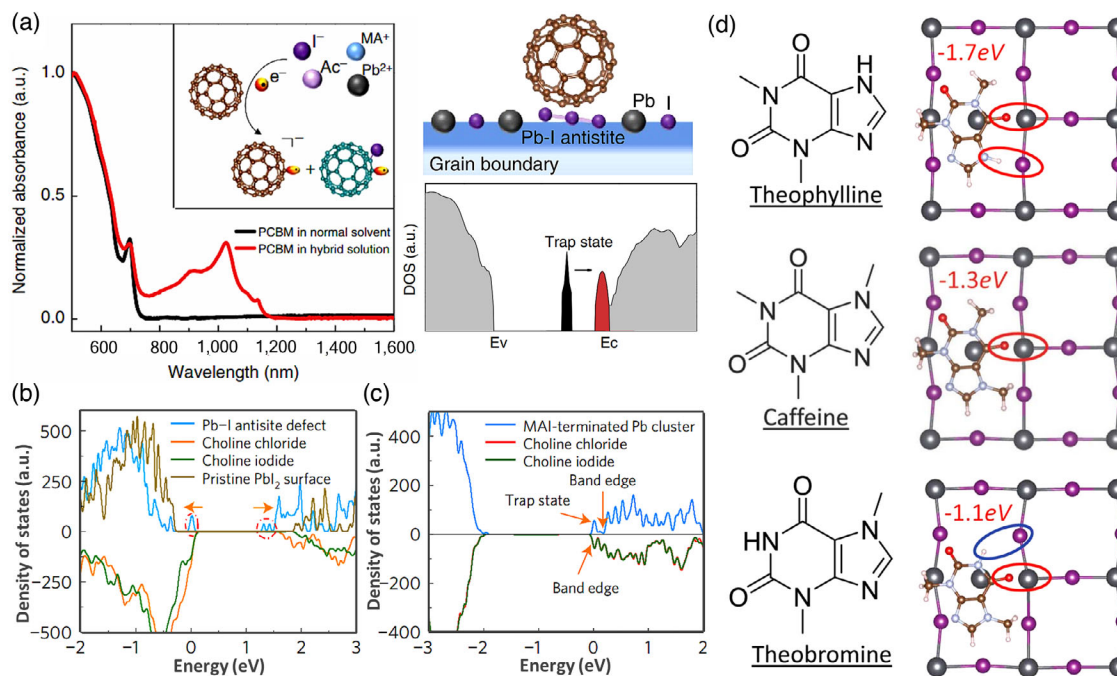


Figure 5. a) UV-vis absorption spectroscopy of perovskite-PCBM hybrid process. A schematic of in situ passivation of Pb-I antisite defect as well as the density functional theory (DFT) calculation, indicating the reduction of the deep-level traps (black) induced Pb-I antisite to much shallower (red) states when PCBM adsorbs on Pb-I antisite. Reproduced with permission.^[121] Copyright 2015, Springer Nature. DOS of the b) Pb-I antisite and c) Pb cluster defect passivated with different molecules. Reproduced with permission.^[37] Copyright 2017, Springer Nature. d) Theoretical models of the interaction between Pb_I defects and small molecules including theophylline, caffeine, and theobromine. Reproduced with permission.^[73] Copyright 2019, The American Association for the Advancement of Science.

PbI_3^- defects disappear after choline molecule passivation. As a result, choline molecules with a double passivation effect are a better choice of passivating agents for PSCs.^[37] Wang and coworkers reported for the first time that metal nickel ion (Ni^{2+}) played a significant role in passivating PbI_3^- antisite defects and inhibiting the formation of Pb^0 . During the growth of the perovskite film, Ni^{2+} ions coordinated with N containing lone pair electrons in the MA cations, which caused the ordered arrangement of MA and inhibited the generation of Pb^0 . Also, Ni^{2+} ions could interact with I^- from PbI_3^- antisite defects in grain boundaries, which effectively reduces the density of defect states. Accordingly, the PCE of inverted planar PSC was improved to 20.61% from 17.25%.^[75] Wang et al. discussed the passivation effect of different configurations of N–H and carbonyl (C=O) group in the small molecules on the surface Pb_1 antisite defect. Theophylline, caffeine, and theobromine with the same functional group but different chemical structures were selected to interact with the Pb_1 antisite. As shown in Figure 5d, the C=O bond from theophylline has stable coordination with the antisite Pb, and the N–H group on the adjacent imidazole ring with the I of PbI_2 form H bond. This synergistic effect promotes theophylline to produce the optimal passivation effect. The interaction between caffeine and Pb_1 antisite lacks the assistance of hydrogen bonds, resulting in lower interaction energy. For theobromine, the short distance between the

C=O and the N–H leads to a spatially adverse constructive configuration.^[73]

Antisite defects are a major kind of charge trap and can cause loss by carrier recombination. The PbI_3^- defect with a lone pair of electrons can bond with Lewis acid including metal cations and fullerene derivatives through ion bonds or coordinate bonds to inhibit the formation of antisite defects. Among them, some transition metals equivalent to lead ions can efficiently promote the growth of perovskite grains or release lattice stress by lead substitution or doping effect.^[75,122] Therefore, transition metal elements or alkaline earth elements can be utilized to suppress antisite defects and stabilize perovskite crystals. Further, the quaternary ammonium halides have a better passivation effect than fullerene derivatives (such as PCBM) due to its ability to passivate both anionic and cationic defects in the perovskite film.

2.3. Interstitial Ion Defects

Interstitial iodine defects refer to iodine atoms or ions located on unoccupied lattice sites, which produce deep-level traps in the bandgap of perovskite absorbers.^[123] Interstitial iodine has three main charge states according to its local geometrical structures shown in Figure 6a: 1) a positively charged I_i^+ state that behaves as a deep electron trap; 2) a neutral I_i^0 state; 3) a negative I_i^- state that functions as a deep hole trap.^[124] The minimum energy

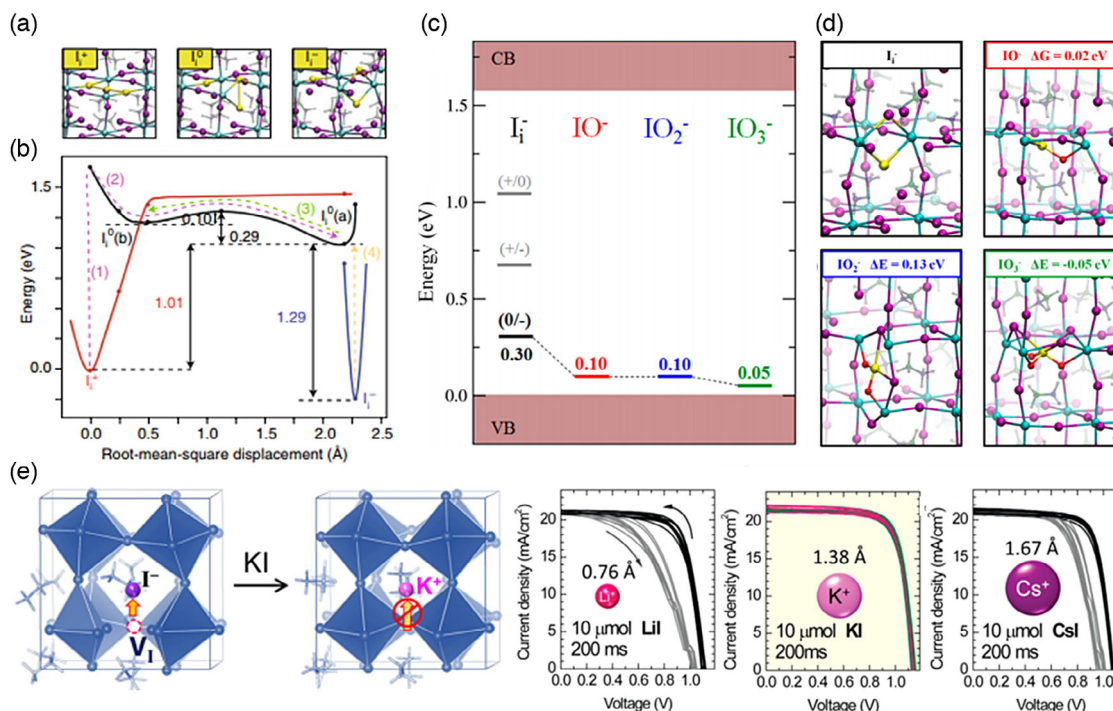


Figure 6. a) Local geometrical structures and b) configuration diagrams of interstitial iodine (I_i) with various charge states. Potential pathways for thermally activated electron trapping (dashed magenta lines, 1, 2), thermally activated electron detrapping (dashed green line, 3), and radiative hole trapping/detrapping (dashed orange line, 4) also illustrated. Reproduced with permission.^[124] Copyright 2018, Springer Nature. c) Thermodynamic ionization levels calculated by Heyd–Scuseria–Ernzerhof spin-orbit coupling of I_i indicating the energetics for hole trapping at I_i^- (0/–, black line); or for electron trapping at I_i^+ (+/0, gray line); or for trapping two-hole or two-electron trapping at I_i^- or I_i^+ , respectively (+/–, gray line). d) Structure of I_i^- and of its interaction products with $1/2 \text{O}_2$, O_2 , and $3/2 \text{O}_2$ along with the calculated energetics (ΔE , eV). Atom color code: yellow, I_i ; purple, I; red, O; light blue, Pb. Reproduced with permission.^[77] Copyright 2017, American Chemical Society. e) J–V curves of PSCs based on perovskite doped with $10 \mu\text{mol}$ of LiI , KI , and CsI . Reproduced with permission.^[76] Copyright 2018, American Chemical Society.

structures of these defects are significantly different. The charge trapping and recombination processes in the perovskite are shown in Figure 6b. Meggiolaro et al. revealed that the unique redox chemistry of the I_i^-/I_i^+ couple dominated the charge capture and decapture process.^[49] And the potentially detrimental hole traps could be transformed into long-living, kinetically inactive electron traps by adjusting the oxidizing conditions during perovskite solution preparation. In addition, a small amount of Br or Cl doping can heal these interstitial iodine sites and turn them into shallow traps.^[49] In another study, Meggiolaro et al. also demonstrated that oxygen was able to oxidize negative interstitial iodine via the formation of moderately stable oxidized complexes (Figure 6c,d), effectively annihilating a source of deep hole traps and reducing the harmful recombination events in the perovskite grains.^[77] Son et al. methodically investigated the inhibitory effect of alkali iodides (lithium iodide [LiI], NaI, KI, rubidium iodide [RbI], or cesium iodide [CsI]) incorporated into bulk perovskite film on the hysteresis of the cells. As can be clearly shown in Figure 6e, I Frenkel defects can be formed by I ion migration to interstitial site and creating iodine vacancies on the lattice site, which is the atomistic origin of hysteresis of perovskite devices. Compared with other alkali cations, K^+ is energetically preferable to occupy interstitial sites, preventing ion diffusion and impeding the formation of Frenkel defects.^[76] KI doping has become a universal method for PSCs with different compositions and structures to reduce hysteresis to a large extent.

The deep-level interstitial I defects can be formed by I ion migration or electron accumulation. Hence, it is a promising method for halide ions with a smaller ion radius or ions that energetically prefer the interstitial sites doping into the perovskite crystals to hinder the migration of I ions to the interstitial sites and convert interstitial defects into shallow-level traps.

2.4. Undercoordinated Pb^{2+}

The intrinsically volatile nature of organic cation is known to occur during the unavoidable thermal annealing in the deposition of OHP films, e.g., MAPbI₃, FAMAPbI₃, due to the low thermal stability of perovskite crystals, which causes the rapid decomposition of perovskite and the formation of the numerous unsaturated Pb²⁺.^[38,125] In addition, the evaporation or oxidation of halide ion can also leave behind the unsaturated Pb²⁺ at the perovskite surface and grain boundaries.^[38,126,127] The uncoordinated Pb²⁺ defects are sensitive to environmental conditions, such as moisture and oxygen, which are likely to form lead oxide and hydroxide when exposed in the air.^[128] In the light of theoretical and experimental studies, the uncoordinated Pb²⁺ defects can result in the generation of trap states in the bandgap^[78,120] that increase charge recombination through nonradiative channels, ion migration under an applied electric field, and water/oxygen permeation, which greatly degrade the efficiency and stability of PSCs.^[79,129,130] Uncoordinated Pb²⁺ ions are capable of accepting electrons, which provides favorable conditions for coordination with Lewis bases. Lewis acids and bases are a kind of typical and effective materials used to passivate undercoordinated sites. The typical Lewis acid/base passivators for uncoordinated ion defects are shown in Table 1.

Lewis bases have the ability to donate electrons and can bind to the electron-deficient defects, forming Lewis complexes by a coordinate covalent bond and eliminating trap recombination centers. The most common examples of Lewis bases are molecules based on the O/N/S donors with lone pair electrons. Noel et al. proposed for the first time that thiophene with S donor and pyridine with N donor for treating perovskite surfaces can effectively passivate the uncoordinated Pb ions and retard the rate of nonradiative recombination, achieving a 3% efficiency improvement.^[80] Later, their derivatives also exhibited a similar passivation effect on defects.^[131] Lin et al. first used a π -conjugated Lewis base IDIC (indacenodithiophene end-capped with 1,1-dicyanomethylene-3-indanone) as an interface layer to reduce trap density on the perovskite films. The IDIC molecules contain C=O and cyano (C≡N) groups that can interact strongly with the uncoordinated Pb ions, yielding a 45% efficiency enhancement in the IDIC-treated PSC.^[78] Therefore, Lewis bases have been increasingly developed as effective passivation molecules for strengthening the photovoltaic performance of PSCs.

Lewis bases containing O donors possess lone pairs of electrons and can bond with the uncoordinated Pb ions as well. Lee et al. utilized the Lewis base N-methyl-2-pyrrolidone (NMP) with O donor to form a strong FAI × PbI₂ × NMP adduct (Figure 7a-f), prompting the formation of highly uniform and reproducible perovskite films.^[81] Wang and coworkers systematically researched the passivation mechanism of electron-donor/electron-acceptor groups on benzene rings to defects in Figure 7g,h.^[82] The substitution of hydrogen on the benzene ring by an electron-donating group will increase the electron cloud density on the benzene ring and enhance the electron donor ability of the benzene ring. Conversely, the electron-donating group will reduce the electron cloud density on the benzene ring. Therefore, when methoxy ($-CH_3O$) group is linked to the benzene ring, the electrostatic interaction between the benzene ring and the undercoordinated Pb²⁺ with the features of electron acceptors is strengthened, which reduces electron capture on the perovskite surface. This explains why CH₃O-PEAI has a better passivation effect than *p*-nitrophenethylammonium iodide (NO₂-PEAI).^[82] Recently, Yang and coworkers demonstrated that caffeine with the two C=O groups as an additive greatly improved the photovoltaic performance of the device and inhibited the thermal decomposition of the films. From the results of Fourier transform infrared (FTIR) spectra, the C=O stretching peaks of caffeine-perovskite film moved to low frequency. This indicates the C=O bond in caffeine was interacted with the Pb²⁺ ions in MAPbI₃, generating a Lewis acid-base adduct. This strong interaction induces lessened trap states and the more preferably crystal orientation.^[83] Furthermore, Han and coworkers formed a stable perovskite heterojunction structure by depositing a thin layer of chlorinated graphene oxide (Cl-GO) on the Pb-rich perovskite surface, and Cl-GO has high coverage on the surface of perovskite with good contact, as shown in Figure 7i. The strong Pb—O and Pb—Cl bonds were generated between the Cl-GO layer and the Pb-rich perovskite film, which could effectively restrain the decomposition of perovskite films and the generation of defects. The efficiency of the champion device modified by Cl-GO is 21.08% with the V_{oc} of 1.12 V.^[84] In addition, Wang et al. used an easily available organic dye, 5-chloroisatin (Isatin-Cl), to eliminate defects on the perovskite

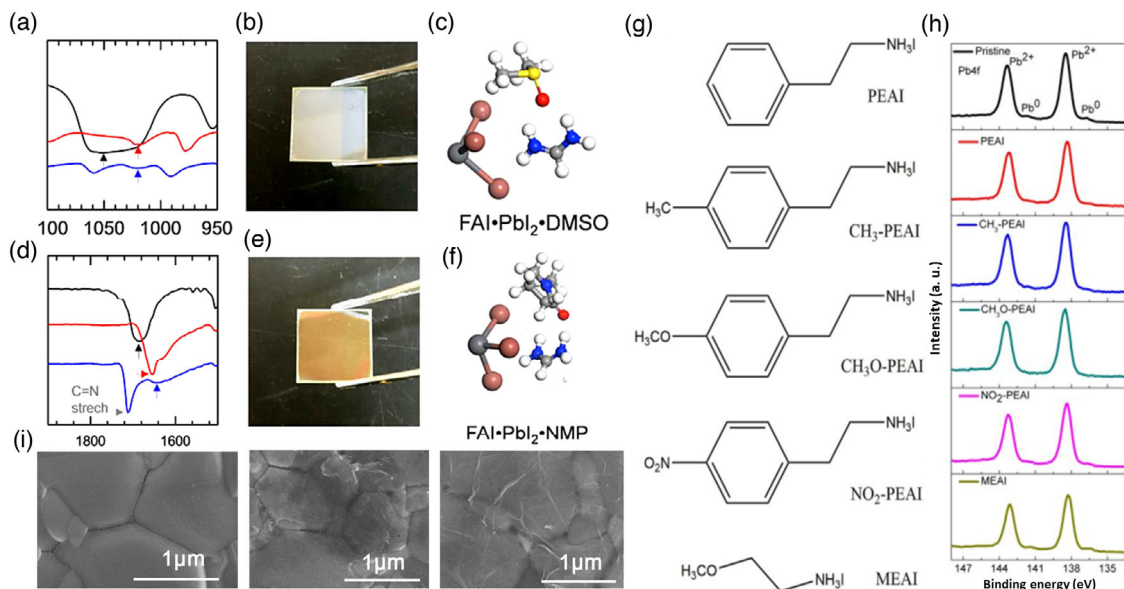


Figure 7. FTIR spectroscopy for a) S=O and d) C=O stretching measured from a) DMSO/d) NMP (solution, black), DMSO/NMP + PbI₂ (powder, red) and DMSO/NMP + PbI₂ + FAI (powder, blue). Photos and molecular structures of b,c) FAI-PbI₂-DMSO and e,f) FAI-PbI₂-NMP adduct films. Reproduced with permission.^[81] Copyright 2018, American Chemical Society. g) The molecular structures of the different organic ammonium iodide salts. h) XPS of Pb 4f core-level spectra. Reproduced with permission.^[82] Copyright 2019, American Chemical Society. i) Top SEM images of the Pb surface-rich perovskite (left), perovskite/GO (center), and perovskite/Cl-GO (right). Reproduced with permission.^[84] Copyright 2019, The American Association for the Advancement of Science.

film surface and along grain boundaries. The chelation between the C=O in Isatin-Cl and uncoordinated Pb²⁺ can effectively reduce the center of nonradiative recombination. Furthermore, the O…H (MA⁺) and the I…H (NH in Isatin-Cl) hydrogen bonds are formed between Isatin-Cl and MAPbI₃, which is beneficial to stabilize the perovskite crystal structure. Therefore, organic dye with favorable functional groups can be used as an excellent material for defective passivator.^[85]

It was reported that the effect of S donor is stronger than that of O donor.^[132] Common S donor Lewis bases mainly include thiophene, thiourea, and their derivatives.^[86–88,133,134] Yang et al. introduced derivatives of thiophene IT-M molecules as Lewis base to successfully passivate the surface defects (the uncoordinated Pb²⁺) by donating electrons, enhancing the photoluminescence (PL) lifetime to 2.2 μs and further raising the PCE up to 20.5% with a FF as high as 0.81.^[88] Ko et al. introduced thiourea as an additive in the MAPbI_xCl_{3-x} precursor solution to boost the performances and stabilities of fully printable PSCs. As shown in Figure 8a, the formation of hydrogen bonds between the amino (—NH₂) groups and I atoms and between S donors and the —NH₂ groups in MAPbI_xCl_{3-x} can make the adjacent perovskite crystals more compactly bonded. Then the formation of Lewis acid–base adducts between Pb and S donors can retard the growth of the perovskite crystals, thereby greatly suppressing the generation of defect states.^[86] In addition, Gao et al. conducted the X-ray photoelectron spectroscopy (XPS) and ²⁰⁷Pb NMR tests (Figure 8b) of perovskite film with and without thiourea and determined that thiourea can form strong Pb–S bond with PbI₂, which is conducive to the passivation of perovskite surface and the enhancement of light, oxygen, and thermal stabilities of perovskite films.^[87] Wang et al. also observed that

adding a moderate quantity of thiourea in perovskite precursor solution can observably enhance the crystal quality and morphology of perovskite films to improve photoelectric characteristics by forming MAI × PbI₂ dimethyl sulfoxide (DMSO) thiourea complexes.^[133]

In another study, Bi et al. proposed a design strategy with a multifunctional molecular modulator for regulating the structure and function of PSCs. As shown in Figure 8c, they designed a bifunctional molecular, namely 3-(5-mercaptop-1H-tetrazol-1-yl) benzenaminium iodide (SN) composed of thiol-based 5-(methylthio)-1H-tetrazole (S) and anilinium iodide (N), of which thiol-functionalized (—SH) interacts with the undercoordinated Pb²⁺ defects, whereas —NH₃⁺ can fill the cation vacancy defects and —NH can form H bonds with the perovskite surface.^[89] The multiple passivation effects of SN provide a new way to achieve highly efficient and stable PSCs. Widely, Feng et al. successfully applied dimethyl sulfide (DS) additive to flexible perovskite solar cells (F-PSCs). A chelated intermediate was formed between DS and Pb²⁺, as shown in Figure 8d, which retards the transformation kinetics during the crystallization process of the perovskite, thereby reducing the defect density. Consequently, the PCE of a small area F-PSC reached 18.40%, and flexible cell with an area of 1.2 cm² achieved a PCE of 13.35%.^[90] Furthermore, Li et al. chose conjugated polymers with molecular fluorination to form a thin protection layer on the surface of perovskite film.^[135] Achieving multiple functions of morphology optimization, surface passivation, and moisture resistance, conjugated polymer materials have significant potential to become a facile and universal strategy to enhance device performance and long-term stability.^[136–138]

Typical molecules of Lewis bases contain pyridine and amino-based molecules. Zuo et al. demonstrated that long-chain

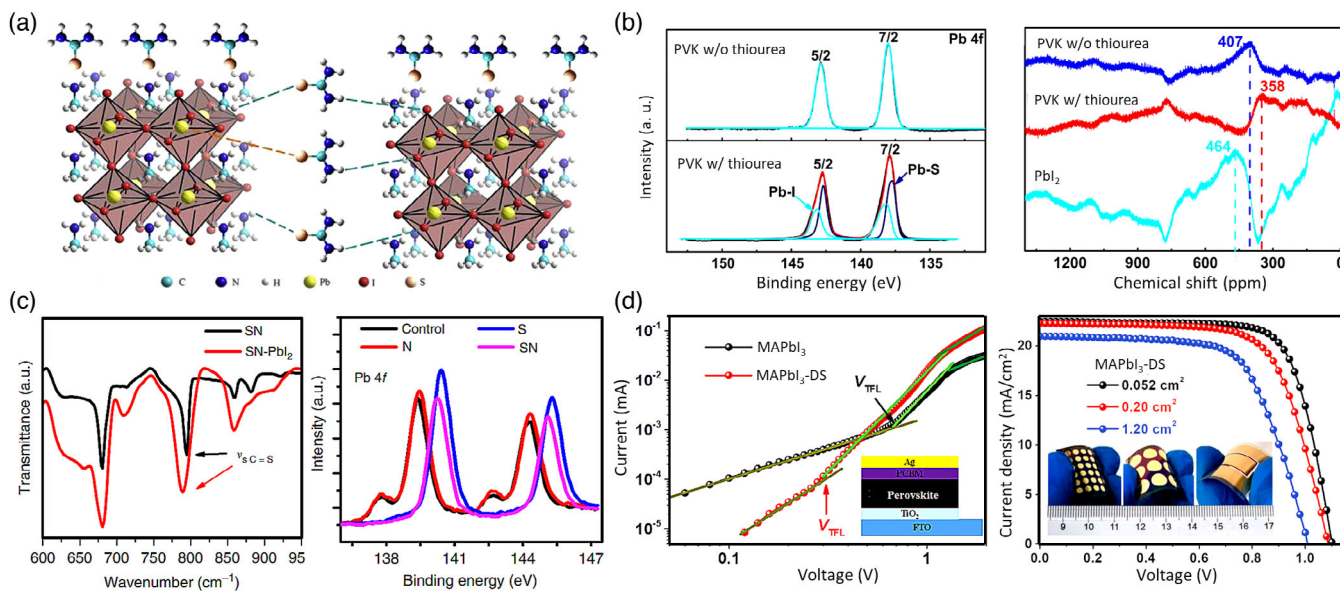


Figure 8. a) Schematic illustration for the effect of thiourea on the growth of perovskite crystals. Reproduced with permission.^[86] Copyright 2019, Elsevier. b) XPS (left) and ²⁰⁷Pb NMR (right) spectra of perovskite film with and without thiourea. Reproduced with permission.^[87] Copyright 2018, John Wiley and Sons. c) FTIR spectra of pure SN and SN–PbI₂ adduct (left). XPS of the perovskite films in the absence (control) and presence of molecular modulators (N, S, and SN) (right). Reproduced with permission.^[89] Copyright 2018, Springer Nature. d) Dark J–V curves of the electron devices. The inset shows the structure of the device (left). J–V curves and photos of different active areas for the MAPbI₃-DS F-PSCs (right). Reproduced with permission.^[90] Copyright 2018, John Wiley and Sons.

polymer additives with different coordinating groups facilitate favorable changes in the optoelectronic performance of the devices by forming coordination bonds with perovskite in Figure 9a. Different binding interactions between the perovskite and the functional groups in molecules can affect the passivation effect of trap states in grain boundaries. The optimal coordinating poly(4-vinylpyridine) (PVP) polymer with Lewis base pyridine has a binding energy of 37.7 kJ mol⁻¹ with Pb²⁺, and polyacrylic acid (PAA) polymer with carboxylic groups has lower coordination energy of 15.71 kJ mol⁻¹, which causes that the passivation effect of PAA is inferior to that of PVP.^[44] Beyond that, Hadadian et al. introduced nitrogen-doped reduced graphene oxide (N-RGO) into halide perovskite precursor solution, which improved all the photovoltaic parameters attributed mainly to the formation of larger grains and the surface-passivation of the film via graphene sheets, as shown in Figure 9b.^[91] Organic ammonium salts have also been reported by Zhu et al. to have similar functions.^[139] They judiciously designed a new passivation molecule, *4-tert*-butyl-benzylammonium iodide (tBBAI) in Figure 9c, that significantly enhanced charge extraction from the perovskite film into hole transport layer (HTL), while suppressing carrier radiationless recombination. In addition, the hydrophobic *tert*-butyl resists the invasion of moisture, leading to better operational stability. As a result, the tBBAI-treated PSC achieved an outstanding PCE of 23.5% with the V_{oc} and FF up to 1.142 V and 0.821, respectively. Wu et al. incorporated bilateral alkylamine (BAA) additives (i.e., 1,3-diaminopropane (DAP), 1,6-diaminohexane (DAH), and 1,8-diaminoctane (DAO)) with –NH₂ terminal groups based on different carbon chain lengths into the perovskite ink in Figure 9d. The –NH₂ tails in the BAAs have the ability to form coordination bonds with the uncoordinated Pb²⁺ to passivate crystal defects at

the grain surface. Also, the –NH₂ groups can fill organic cation vacancies. Other than that, BAAs can form a self-assembled waterproof barrier by exposing the hydrophobic carbon chain. Combining these results, the multifunctional BAAs can construct a uniform and compact perovskite film as well as greatly boost the efficiency and stability of inverted PSCs.^[79]

2.5. Undercoordinated Halide Ions

The uncoordinated halide ions present on the perovskite surface and grain boundaries can serve as charge carrier trap centers.^[80,92] Li et al. investigated that the migration of I⁻ ions or interstitials under the drive of external electrical bias can result in the formation of interfacial barriers at perovskite/Spiro-OMeTAD and TiO₂/perovskite, which impedes the charge injection/extraction and causes the consequent photocurrent hysteresis.^[140] In addition, Liu et al. found that I⁻ ions can migrate through the perovskite grains toward the metal electrode under continuous illumination in nitrogen (N₂), whereas silver (Ag) electrode diffuses toward the HTL, which may lead to the formation of AgI at HTL/metal electrode interface. This is detrimental to carrier behavior and seriously influences device performance.^[141] Therefore, there is an urgent need for effective methods to eliminate these uncoordinated halide ion defects.

Lewis acids usually function as electron acceptors that can combine with the electron-rich defects like uncoordinated halide ions to form a Lewis adduct via coordinated bonding or ionic bonding and passivate undesired deep trap states. Liu et al. used 2-aminoterephthalic acid acting as an additive to inhibit I⁻ ion migration by forming strong coordination with I⁻ ions

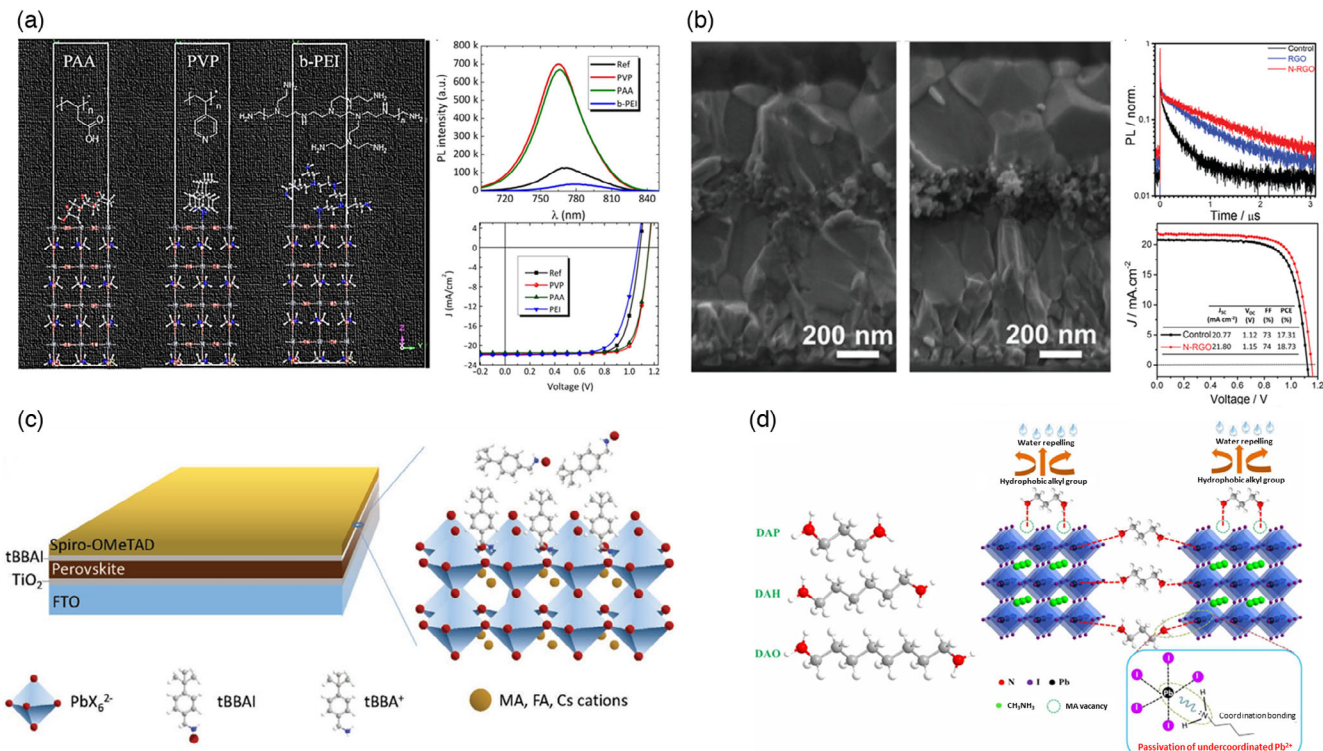


Figure 9. a) The photoelectric properties and J - V curves of the PSCs passivated by branched polyethyleneimine (b-PEI), PAA, and PVP. Reproduced with permission.^[44] Copyright 2017, American Association for the Advancement of Science. b) Cross-sectional SEM images, time-resolved PL decay plots, and J - V characteristics for pristine perovskite (control) and perovskite/N-RGO hybrid solar cell. Reproduced with permission.^[91] Copyright 2016, John Wiley and Sons. c) Structures of a tBBAI-passivated PSC. Reproduced with permission.^[139] Copyright 2020, John Wiley and Sons. d) Chemical structures of BAA additives and schematic illustration of defect passivation and water repellence induced by BAA introduced. Reproduced with permission.^[79] Copyright 2019, American Association for the Advancement of Science.

in the perovskite.^[93] Jiang et al. effectively tuned the quality, photoelectronic properties, and stability of perovskite films via introducing hydroxylamine hydrochloride (HaHc).^[94] The Cl⁻ ions from HaHc can improve the crystallization kinetic of perovskite and reduce the grain boundary. Also, the hydroxyl (—OH) groups in HaHc can form a strong H bond with I⁻ in the perovskite, suppressing the possible degradation of the perovskite film. Abate et al. found that undercoordinated I⁻ ions on the surface of $\text{CH}_3\text{NH}_3\text{PbX}_3$ crystal caused an increase in electron-rich surface defects, which serve as trap sites of holes resulting in the accumulation of holes at the perovskite/Spiro-OMeTAD heterojunction, as shown in Figure 10a–c. In Figure 10d, iodopentafluorobenzene (IPFB) as Lewis acid can strongly interact with undercoordinated I⁻ ions by forming supramolecular halogen bonds, thereby screening electrostatic charges of the uncoordinated I⁻ ions and promoting effective charge transfer at the interface.^[92] The organic molecule guanidinium (GA) can also form hydrogen bonds with undercoordinated iodine species along the grain boundaries, hence effectively passivating the charge trapping/recombination centers. As shown in Figure 10e,f, in the fluorescence intensity mapping of the GA film, the number of dark regions distributed to grain boundary regions is smaller than that of MA film. In addition, from the results in Figure 10g, h, the GA-based film has a stronger fluorescence intensity, indicating that the carrier lifetime is longer, which proves that GA

significantly reduces the interfacial recombination and improves the performance of PSCs.^[95] Meanwhile, Ye et al. discovered that Cu(thiourea)I [Cu(Tu)I] could act as an efficient trap state passivator to be incorporated in perovskite film. The possible passivation mechanism is shown in Figure 10i, and the iodine from Cu(Tu)I can fill the halide vacancy, whereas the positive-electric Cu atoms in Cu(Tu)I are prone to chelate with the undercoordinated halide ions, thereby making the defect energy level shallower and reducing the defect density (Figure 10j). Moreover, the increase in depletion width reveals that the p-type Cu(Tu)I can construct the bulk heterojunction with the ambipolar perovskite, which significantly promotes carrier transport. After Cu(Tu)I passivation, an optimal PCE of 19.9% has been achieved in the inverted PSCs.^[96]

The Pb²⁺ and I⁻ with good coordination ability in perovskite film can be combined with various Lewis acid–base passivators to form complexes, such as salts, organic or inorganic molecules, and polymer molecules. However, under adverse operating conditions such as high humidity or high temperature, small molecule passivators may not be able to maintain interaction with mixed halide perovskite due to their diffusibility and the weak bonding with perovskite crystal. Therefore, polymer molecule passivators with multiple Lewis acid or base groups are a promising strategy for fabricating high-quality perovskite films with low defect density and stable PSCs. Reasonable design

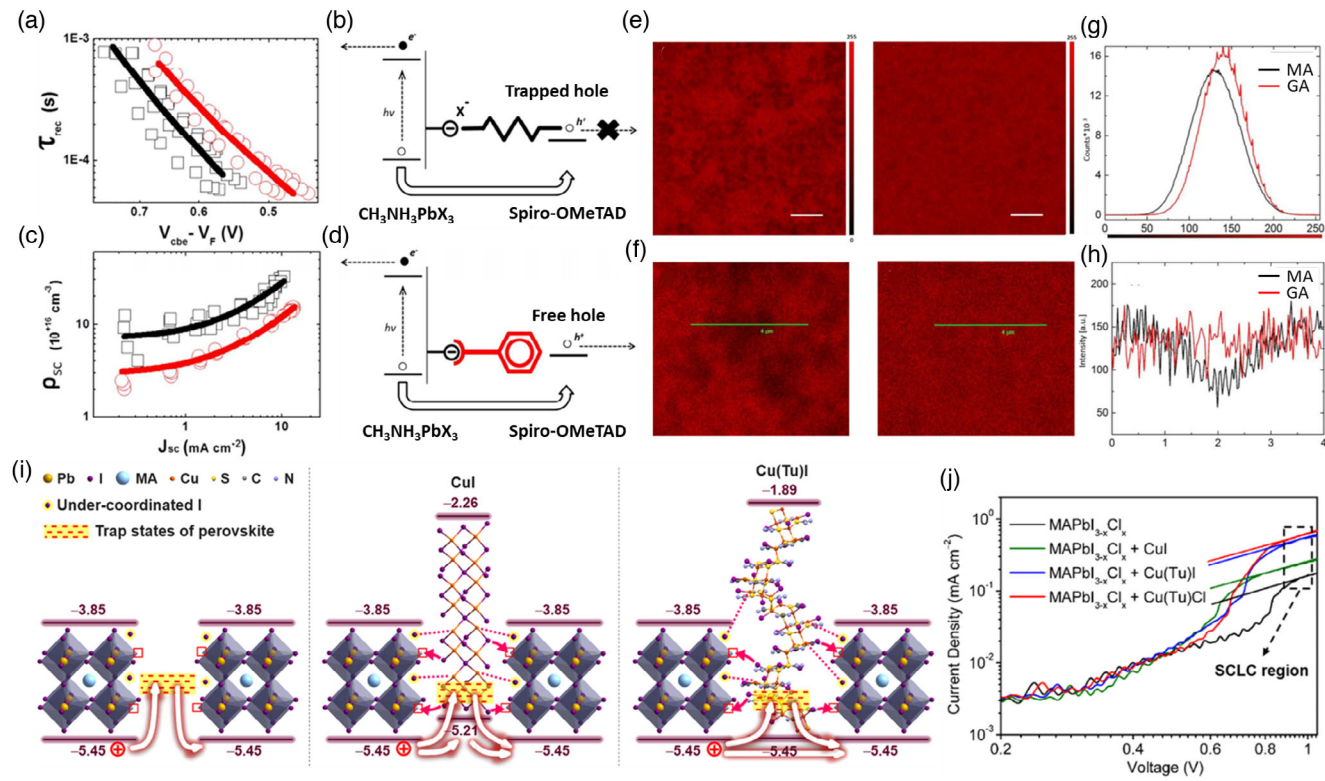


Figure 10. a,c) Photocurrent and photovoltage decay measurements for perovskite-sensitized solar cells (PSSCs) with (red line) or without (black line) IPFB treatment. b) Illustration of the electrostatic interaction between the uncoordinated halide (X^-) and the hole injected in the Spiro-OMeTAD. d) Illustration of the electrostatic screening of the halide (X^-) via halogen bond complexation of IPFB. Reproduced with permission.^[92] Copyright 2014, American Chemical Society. e) Confocal fluorescence intensity images and f) the magnified view for MA (left) and GA (right) (scale bars are 5 and 4 μ m, respectively). g) The intensity range histogram of fluorescence images of MA and GA, respectively. h) Linear intensity profiles. Reproduced with permission.^[95] Copyright 2016, American Chemical Society. i) Schematic illustration of a possible mechanism for the defect passivation. j) J-V curves of the hole-only devices ITO/[poly(3,4-ethylenedioxythiophene):polystyrenesulfonate]/MAPbI_{3-x}Cl_x (without or with trap state passivators)/Au. Reproduced with permission.^[96] Copyright 2017, American Chemical Society.

and synthesis of effective multifunctional passivation molecules will be a research direction in the future.

2.6. Pb⁰/I⁰

Perovskite defects like Pb and I defects are detrimental kinds of carrier traps,^[4,142] which are consistent with that has been observed in other reports.^[114,143,144] Under some aging stresses, such as light irradiation,^[4] moisture,^[145] and thermal stress,^[108] the perovskite material is prone to degradation to generate PbI₂ and other fragments because of its low dissociation energy.^[146] Qin et al. first illuminated the trap-induced degradation mechanism of PSCs. A large number of hole traps were found in the PSC degraded by continuous illumination, and Pb⁰ defects have the potential to form hole traps.^[4] Later, Li et al. reported the decomposition process of MAPbI₃ perovskite under laser irradiation. From the XPS results, the MAPbI₃ film first decomposed into PbI₂ and other volatile fragments, of which PbI₂ sequentially decomposed into Pb and I under further irradiation.^[147] Raga et al. composed the perovskite films annealed in a dry N₂ and in an industrial environment with 50% humidity, respectively, and found that metallic Pb was detected in both samples.^[144] Furthermore, after annealing in the glovebox to crystallize,

Sadoughi et al. optimized the annealing procedures of perovskite film by further annealing in air for 1 h to reduce the concentration of metallic Pb.^[148] What's more, Linddlod and coworkers were inclined to believe that the production of Pb⁰ in the one-step- and two-step-processed TiO₂/MAPbI₃ may be related to the loss of I atom in the form of I₂.^[149,150] In later research, it was noticed that the poly(methyl methacrylate) (PMMA)-treated perovskite lattice had a low content of I vacancies, which indicated a low level of Pb species in the perovskite film.^[151] The metallic Pb is not only a deep defect state that has an adverse effect on the PSCs,^[152] but also a quenching center of excitons that reduces the PL quantum efficiency.^[148,153] In contrast, I⁰ can be oxidized to I⁰. Wang et al. showed that I₂ vapor exerted an accelerated degradation effect on MAPbI₃ perovskite. I⁰ was generated from a series of chemical reactions due to I₂ vapor exposure.^[114] Bischak et al. proposed that light-induced phase separation of halide hybrid perovskites formed an iodide-rich cluster localized at grain boundaries to hamper the improvement of device efficiency.^[154] Therefore, it is vital to eliminate Pb⁰ and I⁰ defects to prepare the perovskite film with perfect electronic quality.

Zhang et al. proved that hypophosphorous acid (HPA) as an additive could reduce the defects density of Pb⁰ and I vacancies

caused by the unbalanced stoichiometry of I/Pb.^[97] Wang et al. introduced europium acetylacetone [Eu(acac)₃] as the source of Eu³⁺-Eu²⁺ ion pair into the perovskite solution,^[98] which substantially inhibited the degradation of the device. As shown in Figure 11a, in the whole system, perovskite inevitably degrades under some excitation stresses, resulting in the generation of Pb⁰ and I⁰ defects. Eu³⁺ can easily oxidize metallic Pb⁰ to Pb²⁺, whereas Eu²⁺ can simultaneously reduce I⁰ to I⁻. In the process of defect elimination, both Eu³⁺ and Eu²⁺ will be regenerated as products, following up the next cycle. The europium-ion pair suppresses Pb⁰ and I⁰ defects at the same time, which achieved the optimized PCE up to 21.52% (certified 20.52%) with enhanced long-term stability. In addition, it has been reported that benzoquinone (BQ), functioning as a commonly used weak oxidizing agent, can effectively eliminate metallic Pb in PbS quantum dots film to inhibit the sub-bandgap states.^[155] Qin et al. utilized the interaction between MAI and BQ to retard the crystallization rate of perovskite and modulate the morphology of the MAPbI₃ film. Further, from the time-of-flight secondary-ion mass spectrometry (TOF-SIMS) image in Figure 11b,c, as the metallic Pb could be oxidized by BQ with oxidation nature, the Pb component in the PSC treated by BQ was obviously suppressed.^[99] A multiple-ligand molecule, pentaerythritol tetrakis (3-mercaptopropionate) (ML) with Lewis basic properties, can not only successfully passivate uncoordinated Pb²⁺, in which the SH ligands interact with PbI₂, but also effectively inhibit the production of metallic Pb⁰.^[100] As shown in XPS images in Figure 11d,e, after several consecutive scans, Pb⁰ species is not clearly observed on the surface of perovskite modified by ML molecule compared with the control group, which is attributed to the oxidation of Pb⁰ to Pb²⁺ by the disulfide intermediate compound formed by the interconnection of two SH groups,

reducing nonradiative recombination. Yang et al. systematically studied the relationship between the structure and function of passivated molecules and engineered a unique amino acid molecule D-4-tert-butyl-phenylalanine (D4TBP) composed of carboxyl, amine, and 4-tert-butylphenyl that has an apparent passivation effect on various defects. It was found that carboxyl and amine could neutralize charged traps due to electrostatic interactions. Moreover, aromatic group could decrease the Lewis acid defects caused by dissociative I, which was supported by toluene added to the iodine-hexane solution to form benzene-iodine complexes in Figure 11f,g.^[101]

Pb⁰ and I⁰ are easily formed under various aging stresses and can act as nonradiative recombination centers to deteriorate the long-term stability of PSCs. Redox-active organic molecules are targeted passivators of Pb⁰ and I⁰ defects to suppress their formation. The oxidant can oxidize Pb⁰ to Pb²⁺ ions, and the reducing agent can reduce I⁰ to I⁻ ions. Therefore, if a redox pair was introduced into the perovskite precursor solution, the cyclic elimination of Pb⁰ and I⁰ defects and the continuous regeneration of the redox shuttle could proceed in succession without introducing additional deep traps. Screening effective redox pairs to synergistically passivate multiple defects is a feasible method to improve carrier extraction capability and enhance device efficiency and lifetime.

3. Ion Migration at Grain Boundary

Defects in the perovskite film can serve as the medium of ion migration. Just as the different pathways for the migration of ions to the perovskite interface are shown in Figure 12a-f.^[156] The ionic nature of the shallow-level point defects allows them to migrate within an electric field due to a lower activation

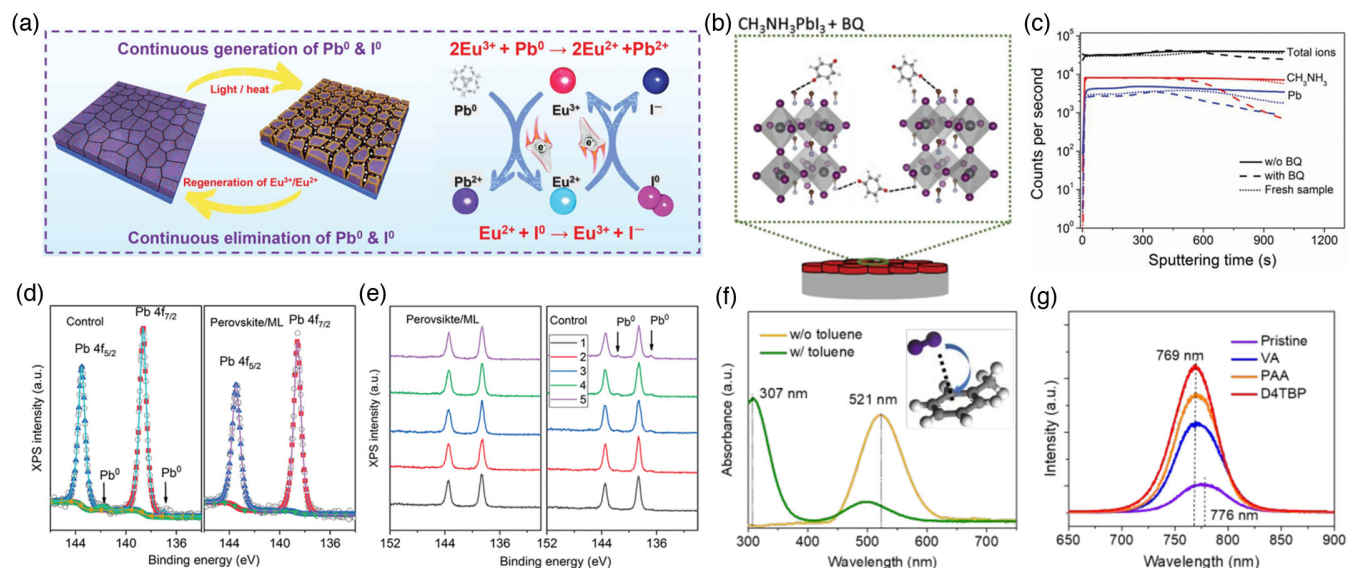


Figure 11. a) The mechanism diagram of cyclical elimination of Pb⁰ and I⁰ defects and regeneration of Eu³⁺-Eu²⁺ ion pair. Reproduced with permission.^[98] Copyright 2019, The American Association for the Advancement of Science. b) Proposed perovskite film formation process. c) TOF-SIMS depth profiles of the degraded PSCs after the Au electrode was peeled away using scotch tape. Reproduced with permission.^[99] Copyright 2016, John Wiley and Sons. d) XPS spectra of the Pb 4f core levels of perovskite derived from the first scan. e) The amount of Pb⁰ monitored by XPS during five continuous scans. Reproduced with permission.^[100] Copyright 2020, John Wiley and Sons. f) UV-vis absorption spectra of iodine dissolved in different solvents. g) PL spectra of perovskite films with different passivation layers. Reproduced with permission.^[101] Copyright 2019, American Chemical Society.

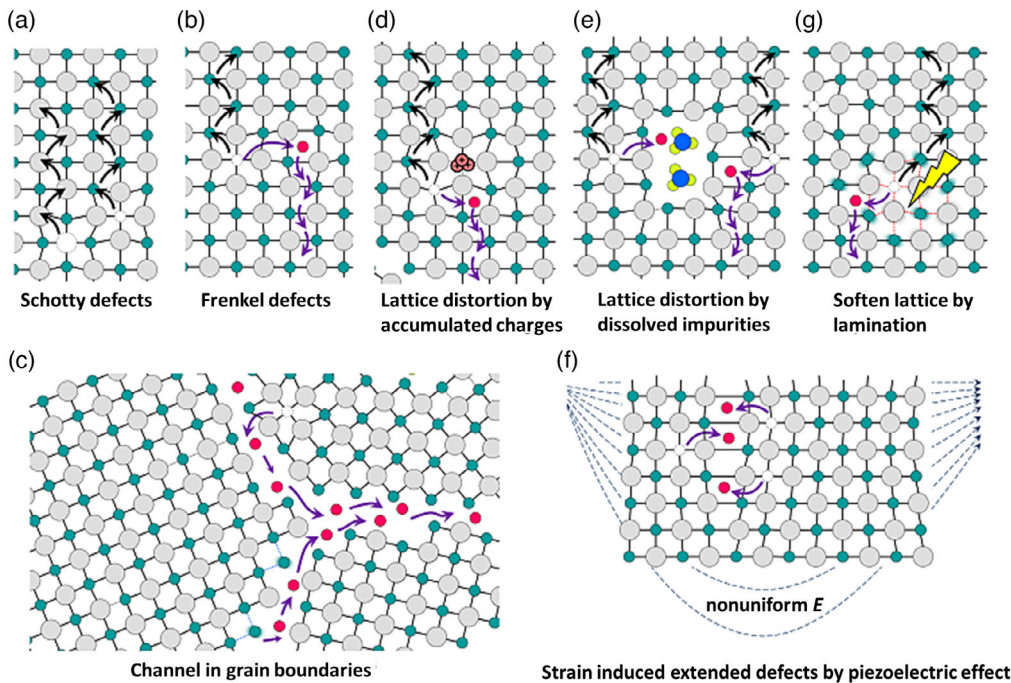


Figure 12. Illustration of the ion migration channels enabled by a) Schottky defects, b) Frenkel defects, c) open space and wrong bonds at grain boundaries, d-f) lattice distortions due to d) accumulated charges, e) dissolved impurities, and f) nonuniform strain caused by the piezoelectric effect, and g) Soften lattice caused by light illumination-induced bond weakening. Reproduced with permission.^[156] Copyright 2016, American Chemical Society.

energy. In addition, Shao et al. demonstrated that grain boundaries could act as the dominant channel for ion migration in the polycrystalline perovskite films. Also, ion migration at the boundaries is much faster than at the grain interiors.^[157] In addition, lattice distortion,^[158] strain,^[159] and lattice softness^[160] are also potential channels for ion migration. A large number of studies have observed that MA^+ or I^- ions were capable of migration under illumination or an applied electric field within the perovskite films. The migration of mobile ions may cause many adverse effects including band bending,^[47,50,161] $J\text{-V}$ hysteresis,^[162,163] lattice strain,^[102] reaction with neighboring function layers,^[164–166] and phase segregation,^[154,167,168] thereby seriously impacting the carrier extraction efficiency and the photoelectric performance of PSCs. During the device operation, the photo-generated field inside the PSC may drive the positively (or negatively) charged defects to migrate toward the HTL (or electron transport layer [ETL]). This results in charge accumulation on both sides of perovskite film and thereafter the generation of an internal potential opposite to the photogenerated field, which impedes the carrier transport and extraction.^[50] Photovoltage-driven ion migration probably causes the local n/p-type doping at different interfaces of perovskite layer that induces band bending in OHP film, as shown in Figure 13a,b.^[169] Thus the charge accumulation and local doping resulted from ion migration are likely to form band bending that impacts the carrier collection at the perovskite/carrier transport layer (CTL) interface and causes hysteretic behaviors. Furthermore, Wu et al. found that the voltage-driven MA^+ migration and accumulation at the perovskite interface could cause the increase in lattice strain including lattice distortion and interface bond breaking. Inserting a fullerene

derivative [6,6]-phenyl-C₆₁-butyric acid (PCBA) film can significantly relieve interface stress and reduce the generation of interface defects.^[102] Movable ions that migrate to the device interface may react chemically with neighboring functional layers leading to device degradation.^[50] In addition, the undesirable reaction between I^- in the perovskite film and Spiro-OMeTAD⁺ molecules was observed by Carrillo et al. This caused a decrease in the conductivity of HTL and a deterioration of device performance.^[164] Kato et al. identified that the color change of Ag electrode occurred due to the reaction between the I^- ion and Ag electrode to form AgI that results from I^- migration through the HTL, exerting an adverse effect on PCE.^[166] In addition, ion migration is the origin of phase segregation in OHP thin films under illumination. As early as 2012, Hoke et al. observed the photoinduced halide segregation due to the appearance of a new PL peak for $\text{MAPb}(\text{Br}_{x}\text{I}_{1-x})_3$ thin film under 1-sun illumination.^[168] More recently, Zhou et al. utilized in situ PL technique and galvanostatic measurement for the first time to confirm the existence of phase separation and ion migration in CsFAMA perovskite layer under the simultaneous irradiation of electric field and light (Figure 13c,d). They further proposed that CsPbBr_3 clusters located on the perovskite surface/interface have the ability to passivate defect states and increase the ion migration energy, yielding an excellent PCE of 20.6% in planar TiO_2 -based CsFAMA PSCs.^[103] These studies emphasize the significance of hindering the migration of mobile ions to promote the efficiency and stability of PSCs.

Widely used methods to suppress ion migration are the passivation of surface and grain boundary and grain modulation, as shown in Table 1. On the one hand, passivation of the

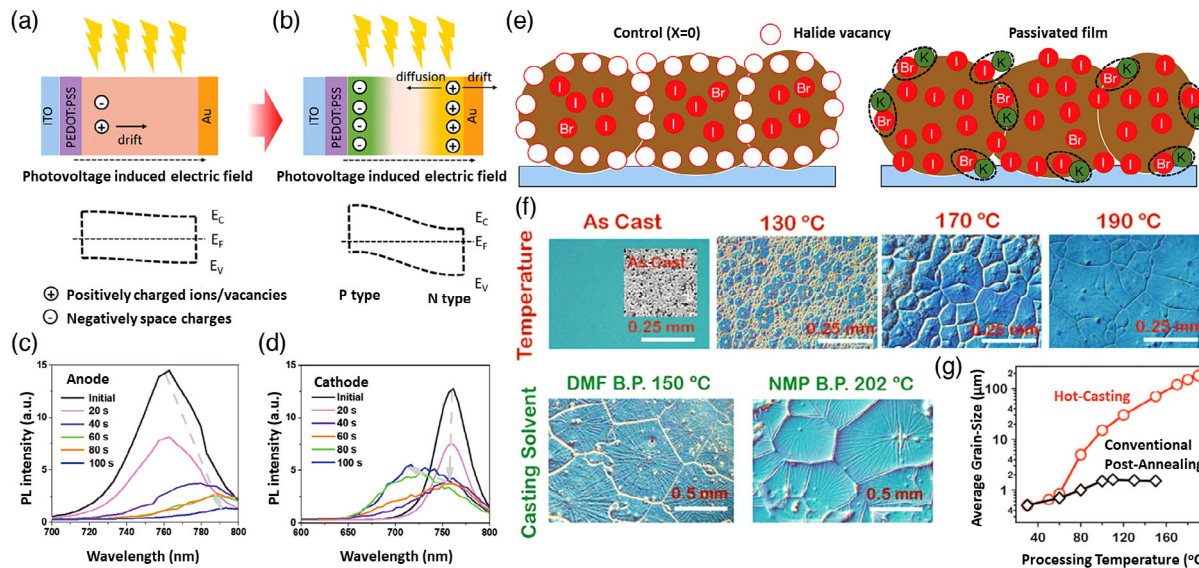


Figure 13. Schematics showing the light-induced self-poling (LISP) process in PSCs and the energy diagram in perovskite layer a) before and b) after. Reproduced with permission.^[169] Copyright 2015, John Wiley and Sons. PL spectra at the c) positive pole and d) negative pole after different electric poling durations. Reproduced with permission.^[103] Copyright 2019, John Wiley and Sons. e) Schematics of halide-vacancy management in cases of excess halide in perovskite film. Reproduced with permission.^[69] Copyright 2018, Springer Nature. f) Optical micrographs showing grain formation as a function of substrate temperature and the boiling points of solvents. g) Comparison of grain size as a function of processing temperature obtained for the hot-casting and conventional post-annealing methods. Reproduced with permission.^[170] Copyright 2015, The American Association for the Advancement of Science.

perovskite surface and grain boundaries to eliminate channels for ion migration is crucial for reducing charge trapping, mitigating photocurrent hysteresis, and enhancing device stability.^[171] Shao et al. found that large and nonmobile fullerene molecules can physically block the ion migration by filling the grain boundaries and coating perovskite surfaces.^[157] And layered perovskites have also been found to suppress the ion migration through the formation of a physical barrier.^[104] Wang et al. regulated the content of *n*-butylammonium incorporated into 3D perovskite, which induced the formation of 2D-phase perovskite crystallites embedded between 3D perovskite grains, leading to improved crystallinity and passivated interfacial grain boundaries responsible for nonradiative charge recombination. Shao et al. developed a new MAPbI₃-TiO₂ composite film to achieve the passivation of grain boundary by simply depositing a mixed precursor solution of MAPbI₃ and TiO₂ nanoparticles. TiO₂ nanoparticles accumulated at grain boundaries with the properties of quick extraction and reservation of photogenerated electron can retard the nonradiative recombination and reduce energy loss, promoting V_{oc} and FF. Meanwhile, the strong bindings between I atoms of perovskite and Ti atoms are able to suppress I ion migration along the grain boundaries, which is beneficial to improve device stability and minimize photocurrent hysteresis.^[105] In addition to the aforementioned passivation by the fullerene, Zhao et al. found that PCBM was capable of inhibiting ion movement through the formation of a donor-acceptor complex with uncoordinated atoms on the surface of the absorber layer. Later, PCBM is also able to chemically absorb on the top of thin films, which greatly diminishes hysteresis in the TiO₂ n-i-p planar structure.^[106] In another research, Abdi-Jalebi et al. used a passivating KI layer to modify the perovskite surface and grain boundaries, as shown in Figure 12e.

Excess iodide can fill any halide vacancies, thereby blocking the nonradiative recombination channel of carriers and generating the high luminescence yields.^[69] The surplus halides immobilized at the grain boundaries and surface make for hindering ionic migration and suppressing additional recombination loss. On the other hand, modulating the crystallization and growth of perovskite to form large-sized grains is also a feasible strategy to reduce grain boundaries and restrain ion migration. Li et al. incorporated Cs⁺ into perovskite film to enlarge grain size, which was explained that cesium chloride (CsCl) in PbI₂ solution containing perovskite seeds could decrease nucleation sites and slow the growth rate of perovskite. Ultimately, the PSCs with CsCl additives showed an outstanding average efficiency of 21.3%.^[107] Nie et al. observed the formation of grains in the case of high substrate temperatures or using high boiling point solvents (Figure 13f,g). Thus, they developed a solution-processed hot-casting technique to form hysteresis-free PSCs with millimeter-scale grains.^[170]

Ion migration is mediated by defects in perovskite film and is an internal factor affecting the stability of PSCs. Therefore, the passivation of the perovskite surface and grain boundaries can effectively suppress the migration of movable ions. Both fullerenes and LD-layered perovskites can serve as physical barriers to spatially block ion migration. In addition, fullerene can also be used as defect passivators and surface modification layer. The LD perovskite can effectively protect the 3D perovskite layer from moisture invasion to improve operation stability. These two passivation techniques are simple and direct ways to mitigate ion migration. Further, the grain modulation essentially eliminates the channels for ion migration. Controlling the nucleation and crystallization processes of perovskite crystals through the modulation of anions or cations and new crystal growth technologies

to form perovskite thin films with large-sized grains and high crystallinity are conducive to improve the overall efficiency of the PSCs. Therefore, studies on the crystallization kinetics of perovskite growth to reduce grain boundaries are greatly needed to eliminate ion migration.

4. Conclusion

To realize the commercialization of PSCs, it is necessary to synergistically exploit high-performance PSCs with improved operational stability. Though the PCE of PSCs has exceeded 25%, its long-term stability is still a huge challenge that limits the rapid development of PSCs. Therefore, a deeper understanding of the defect chemistry at the perovskite surface/interface and the mechanism of device deterioration is urgently required.

Here, we systematically discussed the possible formation causes of various defects (vacancies, antisite defects, interstitial ions, uncoordinated ions, and Pb^0/I^0) and ion migration on the perovskite surface and grain boundaries. We also summarized the targeted passivation techniques and materials for specific defects, with particular emphasis on their functioning mechanism. Despite most point defects produce shallow energy levels near band edges, their migration can affect the performance of PSCs. Moreover, the deep-level traps from grain boundaries and surface defects can give rise to nonradiative recombination and influence carrier extraction efficiency. Ion migration can actually be understood as the migration of defects in perovskite films, which possibly cause many detrimental impacts such as band bending, hysteresis, lattice strain, device degradation, and phase segregation. Passivation of these defects has played a huge role in reducing energy loss and improving device performance. For instance, metal halides and ammonium halides can fill vacancy defects through ionic or hydrogen bonding. Organic or inorganic molecules and polymers with specific functional groups such as Lewis acids and bases can effectively passivate deep-level traps through coordinate bonding to increase V_{oc} . Oxidant and reductant can greatly suppress the formation of Pb^0 and I^0 . Grain boundary passivation and grain modulation can eliminate the pathways of ion migration by reducing defect density, forming physical barriers or generating large-sized grains.

At present, the characterizations of types and density of defects in various perovskite films are still limited, and the understanding of passivation mechanisms also is insufficient. Moving forward, more advanced characterization techniques and theoretical calculations need to be developed to explore defect chemistry. The relationship between the structure of specific functional groups and the ability to passivate defects also requires to be comprehensively studied to effectively guide the design of passivation molecules and further improve the PCE and stability of PSCs.

Acknowledgements

This work was financially supported by the National Key R&D Program of China (grant no. 2018YFB1500105), National Natural Science Foundation of China (grant nos. 61874167 and 61674084), Fundamental Research Funds for Central Universities of China, the Natural Science Foundation of Tianjin City (17JCYBJC41400), the Open Fund of the Key

Laboratory of Optical Information Science & Technology of Ministry of Education of China (2017KF014); and the 111 Project (B16027), the International Cooperation Base (2016D01025), Tianjin International Joint Research and Development Center.

Conflict of Interest

The authors declare no conflict of interest.

Keywords

defects, nonradiative recombination, passivation, perovskite solar cells, stabilities

Received: June 15, 2020

Revised: July 24, 2020

Published online:

- [1] X. Li, D. Bi, C. Yi, J. D. Decoppet, J. Luo, S. M. Zakeeruddin, A. Hagfeldt, M. Gratzel, *Science* **2016**, 353, 58.
- [2] T. Wang, B. Daiber, J. M. Frost, S. A. Mann, E. C. Garnett, A. Walsh, B. Ehrler, *Energy Environ. Sci.* **2017**, 10, 509.
- [3] D. Bi, W. Tress, M. I. Dar, P. Gao, J. Luo, C. Renevier, K. Schenk, A. Abate, F. Giordano, J.-P. Correa Baena, J.-D. Decoppet, S. M. Zakeeruddin, M. K. Nazeeruddin, M. Grätzel, A. Hagfeldt, *Sci. Adv.* **2016**, 2, e1501170.
- [4] C. Qin, T. Matsushima, T. Fujihara, W. J. Potscavage Jr., C. Adachi, *Adv. Mater.* **2016**, 28, 466.
- [5] Q. Dong, Y. Fang, Y. Shao, P. Mulligan, J. Qiu, L. Cao, J. Huang, *Science* **2015**, 347, 967.
- [6] <https://www.nrel.gov/pv/cell-efficiency.html> (accessed: May 2020).
- [7] A. Kojima, K. Teshima, Y. Shirai, T. Miyasaka, *J. Am. Chem. Soc.* **2009**, 131, 6050.
- [8] H. S. Kim, C. R. Lee, J. H. Im, K. B. Lee, T. Moehl, A. Marchioro, S. J. Moon, R. Humphry-Baker, J. H. Yum, J. E. Moser, M. Gratzel, N. G. Park, *Sci. Rep.* **2012**, 2, 591.
- [9] B. Lee, C. C. Stoumpos, N. Zhou, F. Hao, C. Malliakas, C.-Y. Yeh, T. J. Marks, M. G. Kanatzidis, R. P. H. Chang, *J. Am. Chem. Soc.* **2014**, 136, 15379.
- [10] N. J. Jeon, J. H. Noh, Y. C. Kim, W. S. Yang, S. Ryu, S. I. Seok, *Nat. Mater.* **2014**, 13, 897.
- [11] N. J. Jeon, H. Na, E. H. Jung, T.-Y. Yang, Y. G. Lee, G. Kim, H.-W. Shin, S. Il Seok, J. Lee, J. Seo, *Nat. Energy* **2018**, 3, 682.
- [12] E. H. Jung, N. J. Jeon, E. Y. Park, C. S. Moon, T. J. Shin, T. Y. Yang, J. H. Noh, J. Seo, *Nature* **2019**, 567, 511.
- [13] B. Chaudhary, A. Kulkarni, A. K. Jena, M. Ikegami, Y. Udagawa, H. Kunugita, K. Ema, T. Miyasaka, *ChemSusChem* **2017**, 10, 2473.
- [14] H. Kim, S. U. Lee, D. Y. Lee, M. J. Paik, H. Na, J. Lee, S. I. Seok, *Adv. Energy Mater.* **2019**, 9, 1902740.
- [15] L. K. Ono, Y. Qi, S. Liu, *Joule* **2018**, 2, 1961.
- [16] G. Niu, X. Guo, L. Wang, *J. Mater. Chem. A* **2015**, 3, 8970.
- [17] H. S. Kim, J. Y. Seo, N. G. Park, *ChemSusChem* **2016**, 9, 2528.
- [18] N. Aristidou, I. Sanchez-Molina, T. Chotchuangchutchaval, M. Brown, L. Martinez, T. Rath, S. A. Haque, *Angew. Chem., Int. Ed. Engl.* **2015**, 54, 8208.
- [19] L. A. Frolova, N. N. Dremova, P. A. Troshin, *Chem. Commun.* **2015**, 51, 14917.
- [20] Z. Ni, C. Bao, Y. Liu, Q. Jiang, W. Q. Wu, S. Chen, X. Dai, B. Chen, B. Hartweg, Z. Yu, Z. Holman, J. Huang, *Science* **2020**, 367, 1352.
- [21] W.-J. Yin, T. Shi, Y. Yan, *Appl. Phys. Lett.* **2014**, 104, 063903.

- [22] K. X. Steirer, P. Schulz, G. Teeter, V. Stevanovic, M. Yang, K. Zhu, J. J. Berry, *ACS Energy Lett.* **2016**, *1*, 360.
- [23] A. Walsh, D. O. Scanlon, S. Chen, X. G. Gong, S. H. Wei, *Angew. Chem., Int. Ed. Engl.* **2015**, *54*, 1791.
- [24] X. Wu, M. T. Trinh, D. Niesner, H. Zhu, Z. Norman, J. S. Owen, O. Yaffe, B. J. Kudisch, X. Y. Zhu, *J. Am. Chem. Soc.* **2015**, *137*, 2089.
- [25] R. Long, J. Liu, O. V. Prezhdo, *J. Am. Chem. Soc.* **2016**, *138*, 3884.
- [26] K. Domanski, J. P. Correa-Baena, N. Mine, M. K. Nazeeruddin, A. Abate, M. Saliba, W. Tress, A. Hagfeldt, M. Gratzel, *ACS Nano* **2016**, *10*, 6306.
- [27] Z. Li, C. Xiao, Y. Yang, S. P. Harvey, D. H. Kim, J. A. Christians, M. Yang, P. Schulz, S. U. Nanayakkara, C.-S. Jiang, J. M. Luther, J. J. Berry, M. C. Beard, M. M. Al-Jassim, K. Zhu, *Energy Environ. Sci.* **2017**, *10*, 1234.
- [28] S. Liu, Y. Guan, Y. Sheng, Y. Hu, Y. Rong, A. Mei, H. Han, *Adv. Energy Mater.* **2020**, *10*, 1902492.
- [29] J. M. Ball, A. Petrozza, *Nat. Energy* **2016**, *1*, 16149.
- [30] E. Aydin, M. De Bastiani, S. De Wolf, *Adv. Mater.* **2019**, *31*, e1900428.
- [31] T. H. Han, S. Tan, J. Xue, L. Meng, J. W. Lee, Y. Yang, *Adv. Mater.* **2019**, *31*, e1803515.
- [32] B. Chen, P. N. Rudd, S. Yang, Y. Yuan, J. Huang, *Chem. Soc. Rev.* **2019**, *48*, 3842.
- [33] K. Tvingstedt, O. Malinkiewicz, A. Baumann, C. Deibel, H. J. Snaith, V. Dyakonov, H. J. Bolink, *Sci. Rep.* **2014**, *4*, 6071.
- [34] W. Tress, N. Marinova, O. Inganäs, M. K. Nazeeruddin, S. M. Zakeeruddin, M. Graetzel, *Adv. Energy Mater.* **2015**, *5*, 1400812.
- [35] T. S. Sherkar, C. Momblona, L. Gil-Escríg, J. Avila, M. Sessolo, H. J. Bolink, L. J. A. Koster, *ACS Energy Lett.* **2017**, *2*, 1214.
- [36] C. Xin, J. Zhang, X. Zhou, L. Ma, F. Hou, B. Shi, S. Pan, B. Chen, P. Wang, D. Zhang, X. Chen, Y. Zhao, A. A. Bakulin, Y. Li, X. Zhang, *ACS Appl. Energy Mater.* **2020**, *3*, 3318.
- [37] X. Zheng, B. Chen, J. Dai, Y. Fang, Y. Bai, Y. Lin, H. Wei, Xiao C. Zeng, J. Huang, *Nat. Energy* **2017**, *2*, 17102.
- [38] Q. Chen, H. Zhou, T. B. Song, S. Luo, Z. Hong, H. S. Duan, L. Dou, Y. Liu, Y. Yang, *Nano Lett.* **2014**, *14*, 4158.
- [39] Y. Shao, Z. Xiao, C. Bi, Y. Yuan, J. Huang, *Nat. Commun.* **2014**, *5*, 5784.
- [40] E. A. Alharbi, A. Y. Alyamani, D. J. Kubicki, A. R. Uhl, B. J. Walder, A. Q. Alanazi, J. Luo, A. Burgos-Caminal, A. Albadri, H. Albrithen, M. H. Alotaibi, J. E. Moser, S. M. Zakeeruddin, F. Giordano, L. Emsley, M. Gratzel, *Nat. Commun.* **2019**, *10*, 3008.
- [41] Q. Jiang, Y. Zhao, X. Zhang, X. Yang, Y. Chen, Z. Chu, Q. Ye, X. Li, Z. Yin, J. You, *Nat. Photonics* **2019**, *13*, 460.
- [42] J. Peng, Y. Wu, W. Ye, D. A. Jacobs, H. Shen, X. Fu, Y. Wan, T. Duong, N. Wu, C. Barugkin, H. T. Nguyen, D. Zhong, J. Li, T. Lu, Y. Liu, M. N. Lockrey, K. J. Weber, K. R. Catchpole, T. P. White, *Energy Environ. Sci.* **2017**, *10*, 1792.
- [43] P. L. Qin, G. Yang, Z. W. Ren, S. H. Cheung, S. K. So, L. Chen, J. Hao, J. Hou, G. Li, *Adv. Mater.* **2018**, *30*, e1706126.
- [44] L. Zuo, H. Guo, D. W. deQuilettes, S. Jariwala, N. De Marco, S. Dong, R. DeBlock, D. S. Ginger, B. Dunn, M. Wang, Y. Yang, *Sci. Adv.* **2017**, *3*, e1700106.
- [45] H. Min, M. Kim, S. U. Lee, H. Kim, G. Kim, K. Choi, J. H. Lee, S. I. Seok, *Science* **2019**, *366*, 749.
- [46] L. Kuai, Y. Wang, Z. Zhang, Y. Yang, Y. Qin, T. Wu, Y. Li, Y. Li, T. Song, X. Gao, L. Wang, B. Sun, *Sol. RRL* **2019**, *3*, 1900053.
- [47] C. Eames, J. M. Frost, P. R. Barnes, B. C. O'Regan, A. Walsh, M. S. Islam, *Nat. Commun.* **2015**, *6*, 7497.
- [48] H. S. Duan, H. Zhou, Q. Chen, P. Sun, S. Luo, T. B. Song, B. Bob, Y. Yang, *Phys. Chem. Chem. Phys.* **2015**, *17*, 112.
- [49] D. Meggiolaro, S. G. Motti, E. Mosconi, A. J. Barker, J. Ball, C. Andrea Riccardo Perini, F. Deschler, A. Petrozza, F. De Angelis, *Energy Environ. Sci.* **2018**, *11*, 702.
- [50] J. M. Azpiroz, E. Mosconi, J. Bisquert, F. De Angelis, *Energy Environ. Sci.* **2015**, *8*, 2118.
- [51] M. L. Agiorgousis, Y. Y. Sun, H. Zeng, S. Zhang, *J. Am. Chem. Soc.* **2014**, *136*, 14570.
- [52] H. Yu, H. Lu, F. Xie, S. Zhou, N. Zhao, *Adv. Funct. Mater.* **2016**, *26*, 1411.
- [53] C. Ran, J. Xu, W. Gao, C. Huang, S. Dou, *Chem. Soc. Rev.* **2018**, *47*, 4581.
- [54] A. Buin, P. Pietsch, J. Xu, O. Voznyy, A. H. Ip, R. Comin, E. H. Sargent, *Nano Lett.* **2014**, *14*, 6281.
- [55] A. Buin, R. Comin, J. Xu, A. H. Ip, E. H. Sargent, *Chem. Mater.* **2015**, *27*, 4405.
- [56] W. S. Yang, B. W. Park, E. H. Jung, N. J. Jeon, Y. C. Kim, D. U. Lee, S. S. Shin, J. Seo, E. K. Kim, J. H. Noh, S. I. Seok, *Science* **2017**, *356*, 1376.
- [57] W. J. Yin, T. Shi, Y. Yan, *Adv. Mater.* **2014**, *26*, 4653.
- [58] M. H. Du, *J. Mater. Chem. A* **2014**, *2*, 9091.
- [59] G. J. Wetelaer, M. Scheepers, A. M. Sempre, C. Momblona, J. Avila, H. J. Bolink, *Adv. Mater.* **2015**, *27*, 1837.
- [60] M. I. Saidaminov, J. Kim, A. Jain, R. Quintero-Bermudez, H. Tan, G. Long, F. Tan, A. Johnston, Y. Zhao, O. Voznyy, E. H. Sargent, *Nat. Energy* **2018**, *3*, 648.
- [61] M. Yang, T. Zhang, P. Schulz, Z. Li, G. Li, D. H. Kim, N. Guo, J. J. Berry, K. Zhu, Y. Zhao, *Nat. Commun.* **2016**, *7*, 12305.
- [62] D.-Y. Son, J.-W. Lee, Y. J. Choi, I.-H. Jang, S. Lee, P. J. Yoo, H. Shin, N. Ahn, M. Choi, D. Kim, N.-G. Park, *Nat. Energy* **2016**, *1*, 16081.
- [63] M. Kim, G.-H. Kim, T. K. Lee, I. W. Choi, H. W. Choi, Y. Jo, Y. J. Yoon, J. W. Kim, J. Lee, D. Huh, H. Lee, S. K. Kwak, J. Y. Kim, D. S. Kim, *Joule* **2019**, *3*, 2179.
- [64] F. Wang, W. Geng, Y. Zhou, H. H. Fang, C. J. Tong, M. A. Loi, L. M. Liu, N. Zhao, *Adv. Mater.* **2016**, *28*, 9986.
- [65] Y. Liu, S. Akin, L. Pan, R. Uchida, N. Arora, J. V. Milic, A. Hinderhofer, F. Schreiber, A. R. Uhl, S. M. Zakeeruddin, A. Hagfeldt, M. I. Dar, M. Gratzel, *Sci. Adv.* **2019**, *5*, eaaw2543.
- [66] C. Bi, X. Zheng, B. Chen, H. Wei, J. Huang, *ACS Energy Lett.* **2017**, *2*, 1400.
- [67] N. Li, S. Tao, Y. Chen, X. Niu, C. K. Onwudinanti, C. Hu, Z. Qiu, Z. Xu, G. Zheng, L. Wang, Y. Zhang, L. Li, H. Liu, Y. Lun, J. Hong, X. Wang, Y. Liu, H. Xie, Y. Gao, Y. Bai, S. Yang, G. Brocks, Q. Chen, H. Zhou, *Nat. Energy* **2019**, *4*, 408.
- [68] X. Zheng, Y. Deng, B. Chen, H. Wei, X. Xiao, Y. Fang, Y. Lin, Z. Yu, Y. Liu, Q. Wang, J. Huang, *Adv. Mater.* **2018**, *30*, e1803428.
- [69] M. Abdi-Jalebi, Z. Andaji-Garmaroudi, S. Cacovich, C. Stavrakas, B. Philippe, J. M. Richter, M. Alsari, E. P. Booker, E. M. Hutter, A. J. Pearson, S. Lilliu, T. J. Savenije, H. Rensmo, G. Divitini, C. Ducati, R. H. Friend, S. D. Stranks, *Nature* **2018**, *555*, 497.
- [70] P. Wang, J. Wang, X. Zhang, H. Wang, X. Cui, S. Yuan, H. Lu, L. Tu, Y. Zhan, L. Zheng, *J. Mater. Chem. A* **2018**, *6*, 15853.
- [71] W. Q. Wu, P. N. Rudd, Z. Ni, C. H. Van Brackle, H. Wei, Q. Wang, B. R. Ecker, Y. Gao, J. Huang, *J. Am. Chem. Soc.* **2020**, *142*, 3989.
- [72] M. M. Tavakoli, M. Saliba, P. Yadav, P. Holzhey, A. Hagfeldt, S. M. Zakeeruddin, M. Grätzel, *Adv. Energy Mater.* **2019**, *9*, 1802646.
- [73] R. Wang, J. Xue, K. L. Wang, Z. K. Wang, Y. Luo, D. Fenning, G. Xu, S. Nuryyeva, T. Huang, Y. Zhao, J. L. Yang, J. Zhu, M. Wang, S. Tan, I. Yavuz, K. N. Houk, Y. Yang, *Science* **2019**, *366*, 1509.
- [74] J. Xu, A. Buin, A. H. Ip, W. Li, O. Voznyy, R. Comin, M. Yuan, S. Jeon, Z. Ning, J. J. McDowell, P. Kanjanaboons, J. P. Sun, X. Lan, L. N. Quan, D. H. Kim, I. G. Hill, P. MakSYMovich, E. H. Sargent, *Nat. Commun.* **2015**, *6*, 7081.
- [75] X. Gong, L. Guan, H. Pan, Q. Sun, X. Zhao, H. Li, H. Pan, Y. Shen, Y. Shao, L. Sun, Z. Cui, L. Ding, M. Wang, *Adv. Funct. Mater.* **2018**, *28*, 1804286.

- [76] D. Y. Son, S. G. Kim, J. Y. Seo, S. H. Lee, H. Shin, D. Lee, N. G. Park, *J. Am. Chem. Soc.* **2018**, *140*, 1358.
- [77] D. Meggiolaro, E. Mosconi, F. De Angelis, *ACS Energy Lett.* **2017**, *2*, 2794.
- [78] Y. Lin, L. Shen, J. Dai, Y. Deng, Y. Wu, Y. Bai, X. Zheng, J. Wang, Y. Fang, H. Wei, W. Ma, X. C. Zeng, X. Zhan, J. Huang, *Adv. Mater.* **2017**, *29*, 1604545.
- [79] W. Q. Wu, Z. Yang, P. N. Rudd, Y. Shao, X. Dai, H. Wei, J. Zhao, Y. Fang, Q. Wang, Y. Liu, Y. Deng, X. Xiao, Y. Feng, J. Huang, *Sci. Adv.* **2019**, *5*, eaav8925.
- [80] N. K. Noel, A. Abate, S. D. Stranks, E. S. Parrott, V. M. Burlakov, A. Goriely, H. J. Snaith, *ACS Nano* **2014**, *8*, 9815.
- [81] J. W. Lee, Z. Dai, C. Lee, H. M. Lee, T. H. Han, N. De Marco, O. Lin, C. S. Choi, B. Dunn, J. Koh, D. Di Carlo, J. H. Ko, H. D. Maynard, Y. Yang, *J. Am. Chem. Soc.* **2018**, *140*, 6317.
- [82] J. Zhuang, P. Mao, Y. Luan, X. Yi, Z. Tu, Y. Zhang, Y. Yi, Y. Wei, N. Chen, T. Lin, F. Wang, C. Li, J. Wang, *ACS Energy Lett.* **2019**, *4*, 2913.
- [83] R. Wang, J. Xue, L. Meng, J.-W. Lee, Z. Zhao, P. Sun, L. Cai, T. Huang, Z. Wang, Z.-K. Wang, Y. Duan, J. L. Yang, S. Tan, Y. Yuan, Y. Huang, Y. Yang, *Joule* **2019**, *3*, 1464.
- [84] Y. Wang, T. Wu, J. Barbaud, W. Kong, D. Cui, H. Chen, X. Yang, L. Han, *Science* **2019**, *365*, 687.
- [85] S. Xiong, J. Song, J. Yang, J. Xu, M. Zhang, R. Ma, D. Li, X. Liu, F. Liu, C. Duan, M. Fahrlman, Q. Bao, *Sol. RRL* **2020**, *4*, 1900529.
- [86] S.-G. Ko, G.-I. Ryu, B. Kim, G.-J. Cha, J.-H. Ri, G.-S. Sonu, U.-C. Kim, *Sol. Energy Mater. Sol. Cells* **2019**, *196*, 105.
- [87] L. Gao, S. Huang, L. Chen, X. Li, B. Ding, S. Huang, G. Yang, *Sol. RRL* **2018**, *2*, 1800088.
- [88] G. Yang, P. Qin, G. Fang, G. Li, *Sol. RRL* **2018**, *2*, 1800055.
- [89] D. Bi, X. Li, J. V. Milic, D. J. Kubicki, N. Pellet, J. Luo, T. LaGrange, P. Mettraux, L. Emsley, S. M. Zakeeruddin, M. Gratzel, *Nat. Commun.* **2018**, *9*, 4482.
- [90] J. Feng, X. Zhu, Z. Yang, X. Zhang, J. Niu, Z. Wang, S. Zuo, S. Priya, S. F. Liu, D. Yang, *Adv. Mater.* **2018**, *30*, e1801418.
- [91] M. Hadadian, J. P. Correa-Baena, E. K. Goharshadi, A. Ummadisingu, J. Y. Seo, J. Luo, S. Gholipour, S. M. Zakeeruddin, M. Saliba, A. Abate, M. Gratzel, A. Hagfeldt, *Adv. Mater.* **2016**, *28*, 8681.
- [92] A. Abate, M. Saliba, D. J. Hollman, S. D. Stranks, K. Wojciechowski, R. Avolio, G. Grancini, A. Petrozza, H. J. Snaith, *Nano Lett.* **2014**, *14*, 3247.
- [93] Z. Liu, F. Cao, M. Wang, M. Wang, L. Li, *Angew. Chem., Int. Ed.* **2020**, *132*, 4190.
- [94] H. Jiang, Z. Yan, H. Zhao, S. Yuan, Z. Yang, J. Li, B. Liu, T. Niu, J. Feng, Q. Wang, D. Wang, H. Yang, Z. Liu, S. F. Liu, *ACS Appl. Energy Mater.* **2018**, *1*, 900.
- [95] N. De Marco, H. Zhou, Q. Chen, P. Sun, Z. Liu, L. Meng, E. P. Yao, Y. Liu, A. Schiffer, Y. Yang, *Nano Lett.* **2016**, *16*, 1009.
- [96] S. Ye, H. Rao, Z. Zhao, L. Zhang, H. Bao, W. Sun, Y. Li, F. Gu, J. Wang, Z. Liu, Z. Bian, C. Huang, *J. Am. Chem. Soc.* **2017**, *139*, 7504.
- [97] W. Zhang, S. Pathak, N. Sakai, T. Stergiopoulos, P. K. Nayak, N. K. Noel, A. A. Haghhighirad, V. M. Burlakov, D. W. deQuilettes, A. Sadhanala, W. Li, L. Wang, D. S. Ginger, R. H. Friend, H. J. Snaith, *Nat. Commun.* **2015**, *6*, 10030.
- [98] L. Wang, H. Zhou, J. Hu, B. Huang, M. Sun, B. Dong, G. Zheng, Y. Huang, Y. Chen, L. Li, Z. Xu, N. Li, Z. Liu, Q. Chen, L. D. Sun, C. H. Yan, *Science* **2019**, *363*, 265.
- [99] C. Qin, T. Matsushima, T. Fujihara, C. Adachi, *Adv. Mater.* **2017**, *29*, 1603808.
- [100] Z. Wu, M. Jiang, Z. Liu, A. Jamshaid, L. K. Ono, Y. Qi, *Adv. Energy Mater.* **2020**, *10*, 1903696.
- [101] S. Yang, J. Dai, Z. Yu, Y. Shao, Y. Zhou, X. Xiao, X. C. Zeng, J. Huang, *J. Am. Chem. Soc.* **2019**, *141*, 5781.
- [102] J. Wu, J. Shi, Y. Li, H. Li, H. Wu, Y. Luo, D. Li, Q. Meng, *Adv. Energy Mater.* **2019**, *9*, 1901352.
- [103] W. Zhou, S. Chen, Y. Zhao, Q. Li, Y. Zhao, R. Fu, D. Yu, P. Gao, Q. Zhao, *Adv. Funct. Mater.* **2019**, *29*, 1809180.
- [104] Z. Wang, Q. Lin, F. P. Chmiel, N. Sakai, L. M. Herz, H. J. Snaith, *Nat. Energy* **2017**, *2*, 17135.
- [105] J. Shao, S. Yang, Y. Liu, *ACS Appl. Mater. Interfaces* **2017**, *9*, 16202.
- [106] Y. Zhao, W. Zhou, W. Ma, S. Meng, H. Li, J. Wei, R. Fu, K. Liu, D. Yu, Q. Zhao, *ACS Energy Lett.* **2016**, *1*, 266.
- [107] Q. Li, Y. Zhao, R. Fu, W. Zhou, Y. Zhao, X. Liu, D. Yu, Q. Zhao, *Adv. Mater.* **2018**, *30*, e1803095.
- [108] E. J. Juarez-Perez, Z. Hawash, S. R. Raga, L. K. Ono, Y. Qi, *Energy Environ. Sci.* **2016**, *9*, 3406.
- [109] T. Leijtens, G. E. Eperon, A. J. Barker, G. Grancini, W. Zhang, J. M. Ball, A. R. S. Kandada, H. J. Snaith, A. Petrozza, *Energy Environ. Sci.* **2016**, *9*, 3472.
- [110] D. Barboni, R. A. De Souza, *Energy Environ. Sci.* **2018**, *11*, 3266.
- [111] L.-Y. Wei, W. Ma, C. Lian, S. Meng, *J. Phys. Chem. C* **2017**, *121*, 5905.
- [112] E. Mosconi, D. Meggiolaro, H. J. Snaith, S. D. Stranks, F. De Angelis, *Energy Environ. Sci.* **2016**, *9*, 3180.
- [113] N. Aristidou, C. Eames, I. Sanchez-Molina, X. Bu, J. Kosco, M. S. Islam, S. A. Haque, *Nat. Commun.* **2017**, *8*, 15218.
- [114] S. Wang, Y. Jiang, E. J. Juarez-Perez, L. K. Ono, Y. Qi, *Nat. Energy* **2016**, *2*, 16195.
- [115] T. Niu, J. Lu, M.-C. Tang, D. Barrit, D.-M. Smilgies, Z. Yang, J. Li, Y. Fan, T. Luo, I. McCulloch, A. Amassian, S. Liu, K. Zhao, *Energy Environ. Sci.* **2018**, *11*, 3358.
- [116] D. Bi, P. Gao, R. Scopelliti, E. Oveisi, J. Luo, M. Grätzel, A. Hagfeldt, M. K. Nazeeruddin, *Adv. Mater.* **2016**, *28*, 2910.
- [117] Y. Zhang, G. Grancini, Z. Fei, E. Shirzadi, X. Liu, E. Oveisi, F. F. Tirani, R. Scopelliti, Y. Feng, M. K. Nazeeruddin, P. J. Dyson, *Nano Energy* **2019**, *58*, 105.
- [118] Z. Tang, S. Uchida, T. Bessho, T. Kinoshita, H. Wang, F. Awai, R. Jono, M. M. Maitani, J. Nakazaki, T. Kubo, H. Segawa, *Nano Energy* **2018**, *45*, 184.
- [119] P. N. Rudd, J. Huang, *Trends Anal. Chem.* **2019**, *1*, 394.
- [120] D. W. deQuilettes, S. M. Vorpahl, S. D. Stranks, H. Nagaoka, G. E. Eperon, M. E. Ziffer, H. J. Snaith, D. S. Ginger, *Science* **2015**, *348*, 683.
- [121] C. Z. Li, C. C. Chueh, F. Ding, H. L. Yip, P. W. Liang, X. Li, A. K. Jen, *Adv. Mater.* **2013**, *25*, 4425.
- [122] X. Shai, J. Wang, P. Sun, W. Huang, P. Liao, F. Cheng, B. Zhu, S. Y. Chang, E. P. Yao, Y. Shen, L. Miao, Y. Yang, M. Wang, *Nano Energy* **2018**, *48*, 117.
- [123] M. H. Du, *J. Phys. Chem. Lett.* **2015**, *6*, 1461.
- [124] L. Martiradonna, *Nat. Mater.* **2018**, *17*, 377.
- [125] Y. Yang, J. You, *Nature* **2017**, *544*, 155.
- [126] C. Bi, Y. Shao, Y. Yuan, Z. Xiao, C. Wang, Y. Gao, J. Huang, *J. Mater. Chem. A* **2014**, *2*, 18508.
- [127] A. Dualeh, N. Tétreault, T. Moehl, P. Gao, M. K. Nazeeruddin, M. Grätzel, *Adv. Funct. Mater.* **2014**, *24*, 3250.
- [128] Y. Itzhaik, O. Niitsoo, M. Page, G. Hodes, *J. Phys. Chem. C* **2009**, *113*, 4254.
- [129] B. Yang, O. Dyck, J. Poplawsky, J. Keum, A. Puretzky, S. Das, I. Ivanov, C. Rouleau, G. Duscher, D. Geohegan, K. Xiao, *J. Am. Chem. Soc.* **2015**, *137*, 9210.
- [130] C. Chen, F. Li, L. Zhu, Z. Shen, Y. Weng, Q. Lou, F. Tan, G. Yue, Q. Huang, M. Wang, *Nano Energy* **2020**, *68*, 104313.
- [131] T. Y. Wen, S. Yang, P. F. Liu, L. J. Tang, H. W. Qiao, X. Chen, X. H. Yang, Y. Hou, H. G. Yang, *Adv. Energy Mater.* **2018**, *8*, 1703143.

- [132] I. Wharf, T. Gramstad, R. Makhija, M. Onyszchuk, *Can. J. Chem.* **1976**, *54*, 3430.
- [133] S. Wang, Z. Ma, B. Liu, W. Wu, Y. Zhu, R. Ma, C. Wang, *Sol. RRL* **2018**, *2*, 1800034.
- [134] F. De Angelis, D. Meggiolaro, E. Mosconi, A. Petrozza, M. K. Nazeeruddin, H. J. Snaith, *ACS Energy Lett.* **2017**, *2*, 857.
- [135] F. Li, J. Yuan, X. Ling, Y. Zhang, Y. Yang, S. Cheung, C. Ho, X. Gao, W. Ma, *Adv. Funct. Mater.* **2018**, *28*, 1706377.
- [136] K. Ji, J. Yuan, F. Li, Y. Shi, X. Ling, X. Zhang, Y. Zhang, H. Lu, J. Yuan, W. Ma, *J. Mater. Chem. A* **2020**, *8*, 8104.
- [137] J. Yuan, X. Ling, D. Yang, F. Li, S. Zhou, J. Shi, Y. Qian, J. Hu, Y. Sun, Y. Yang, X. Gao, S. Duham, Q. Zhang, W. Ma, *Joule* **2018**, *2*, 2450.
- [138] F. Li, J. Yuan, X. Ling, L. Huang, N. Rujisamphan, Y. Li, L. Chi, W. Ma, *ACS Appl. Mater. Interfaces* **2018**, *10*, 42397.
- [139] H. Zhu, Y. Liu, F. T. Eickemeyer, L. Pan, D. Ren, M. A. Ruiz-Preciado, B. Carlsen, B. Yang, X. Dong, Z. Wang, H. Liu, S. Wang, S. M. Zakeeruddin, A. Hagfeldt, M. I. Dar, X. Li, M. Grätzel, *Adv. Mater.* **2020**, *32*, e1907757.
- [140] C. Li, S. Tscheuschner, F. Paulus, P. E. Hopkinson, J. Kiessling, A. Kohler, Y. Vaynzof, S. Huettnner, *Adv. Mater.* **2016**, *28*, 2446.
- [141] L. Liu, S. Huang, Y. Lu, P. Liu, Y. Zhao, C. Shi, S. Zhang, J. Wu, H. Zhong, M. Sui, H. Zhou, H. Jin, Y. Li, Q. Chen, *Adv. Mater.* **2018**, *30*, e1800544.
- [142] J. Kim, S. H. Lee, J. H. Lee, K. H. Hong, *J. Phys. Chem. Lett.* **2014**, *5*, 1312.
- [143] B. Conings, L. Baeten, C. De Dobbelaere, J. D'Haen, J. Manca, H. G. Boyen, *Adv. Mater.* **2014**, *26*, 2041.
- [144] S. R. Raga, M.-C. Jung, M. V. Lee, M. R. Leyden, Y. Kato, Y. Qi, *Chem. Mater.* **2015**, *27*, 1597.
- [145] J. M. Frost, K. T. Butler, F. Brivio, C. H. Hendon, M. van Schilfgaarde, A. Walsh, *Nano Lett.* **2014**, *14*, 2584.
- [146] R. K. Gunasekaran, D. Chinnadurai, A. R. Selvaraj, R. Rajendiran, K. Senthil, K. Prabakar, *Chemphyschem* **2018**, *19*, 1507.
- [147] Y. Li, X. Xu, C. Wang, B. Ecker, J. Yang, J. Huang, Y. Gao, *J. Phys. Chem. C* **2017**, *121*, 3904.
- [148] G. Sadoughi, D. E. Starr, E. Handick, S. D. Stranks, M. Gorgoi, R. G. Wilks, M. Bar, H. J. Snaith, *ACS Appl. Mater. Interfaces* **2015**, *7*, 13440.
- [149] R. Lindblad, D. Bi, B. W. Park, J. Oscarsson, M. Gorgoi, H. Siegbahn, M. Odelius, E. M. Johansson, H. Rensmo, *J. Phys. Chem. Lett.* **2014**, *5*, 648.
- [150] G. Niu, W. Li, F. Meng, L. Wang, H. Dong, Y. Qiu, *J. Mater. Chem. A* **2014**, *2*, 705.
- [151] D. Bi, C. Yi, J. Luo, J.-D. Décoppet, F. Zhang, Shaik M. Zakeeruddin, X. Li, A. Hagfeldt, M. Grätzel, *Nat. Energy* **2016**, *1*, 16142.
- [152] B. Philippe, T. J. Jacobsson, J.-P. Correa-Baena, N. K. Jena, A. Banerjee, S. Chakraborty, U. B. Cappel, R. Ahuja, A. Hagfeldt, M. Odelius, H. Rensmo, *J. Phys. Chem. C* **2017**, *121*, 26655.
- [153] H. Cho, S. H. Jeong, M. H. Park, Y. H. Kim, C. Wolf, C. L. Lee, J. H. Heo, A. Sadhanala, N. Myoung, S. Yoo, S. H. Im, R. H. Friend, T. W. Lee, *Science* **2015**, *350*, 1222.
- [154] C. G. Bischak, C. L. Hetherington, H. Wu, S. Aloni, D. F. Ogletree, D. T. Limmer, N. S. Ginsberg, *Nano Lett.* **2017**, *17*, 1028.
- [155] G. W. Hwang, D. Kim, J. M. Cordero, M. W. B. Wilson, C. M. Chuang, J. C. Grossman, M. G. Bawendi, *Adv. Mater.* **2015**, *27*, 4481.
- [156] Y. Yuan, J. Huang, *Acc. Chem. Res.* **2016**, *49*, 286.
- [157] Y. Shao, Y. Fang, T. Li, Q. Wang, Q. Dong, Y. Deng, Y. Yuan, H. Wei, M. Wang, A. Gruverman, J. Shield, J. Huang, *Energy Environ. Sci.* **2016**, *9*, 1752.
- [158] B. Wu, K. Fu, N. Yantara, G. Xing, S. Sun, T. C. Sum, N. Mathews, *Adv. Energy Mater.* **2015**, *5*, 1500829.
- [159] Q. Dong, J. Song, Y. Fang, Y. Shao, S. Ducharme, J. Huang, *Adv. Mater.* **2016**, *28*, 2816.
- [160] R. Gottesman, E. Haltzi, L. Gouda, S. Tirosh, Y. Bouhadana, A. Zaban, E. Mosconi, F. De Angelis, *J. Phys. Chem. Lett.* **2014**, *5*, 2662.
- [161] Y. Yuan, T. Li, Q. Wang, J. Xing, A. Gruverman, J. Huang, *Sci Adv.* **2017**, *3*, e1602164.
- [162] W. Tress, N. Marinova, T. Moehl, S. M. Zakeeruddin, M. K. Nazeeruddin, M. Grätzel, *Energy Environ. Sci.* **2015**, *8*, 995.
- [163] J. Xing, Q. Wang, Q. Dong, Y. Yuan, Y. Fang, J. Huang, *Phys. Chem. Chem. Phys.* **2016**, *18*, 30484.
- [164] J. Carrillo, A. Guerrero, S. Rahimnejad, O. Almora, I. Zarazua, E. Mas-Marza, J. Bisquert, G. Garcia-Belmonte, *Adv. Energy Mater.* **2016**, *6*, 1502246.
- [165] I. M. Hermes, Y. Hou, V. W. Bergmann, C. J. Brabec, S. A. L. Weber, *J. Phys. Chem. Lett.* **2018**, *9*, 6249.
- [166] Y. Kato, L. K. Ono, M. V. Lee, S. Wang, S. R. Raga, Y. Qi, *Adv. Mater. Interfaces* **2015**, *2*, 1500195.
- [167] D. J. Slotcavage, H. I. Karunadasa, M. D. McGehee, *ACS Energy Lett.* **2016**, *1*, 1199.
- [168] E. T. Hoke, D. J. Slotcavage, E. R. Dohner, A. R. Bowring, H. I. Karunadasa, M. D. McGehee, *Chem. Sci.* **2015**, *6*, 613.
- [169] Y. Deng, Z. Xiao, J. Huang, *Adv. Energy Mater.* **2015**, *5*, 1500721.
- [170] W. Nie, H. Tsai, R. Asadpour, J. C. Blancon, A. J. Neukirch, G. Gupta, J. J. Crochet, M. Chhowalla, S. Tretiak, M. A. Alam, H. L. Wang, A. D. Mohite, *Science* **2015**, *347*, 522.
- [171] Y. Zhao, Q. Li, W. Zhou, Y. Hou, Y. Zhao, R. Fu, D. Yu, X. Liu, Q. Zhao, *Sol. RRL* **2019**, *3*, 1800296.



Xin Zhou received her bachelor's degree from China University of Petroleum (East China), in 2018. She is currently a master student at Nankai University under the supervision of Prof. Yuelong Li. Her main research focuses on organic–inorganic halide PSCs.



Yuelong Li is an associate professor at Nankai University since October 2016. He received Ph.D. from the Korea Institute of Science and Technology (KIST/UST), in 2012, and started his postdocs at the University of California-San Diego (UCSD) and then the Spanish National Research Council (CSIC) as a Marie Curie Fellow. He stayed at the University of Oxford (2015) and the University of Cambridge (2018) as a visiting scholar. His research mainly focuses on optoelectronic materials and devices such as dye-sensitized solar cells and PSCs, perovskite/Si tandem solar cells, perovskite single crystals, light-trapping mechanism and structures, and so on.



Xiaodan Zhang is a professor at Nankai University. Her main research interests include 1) perovskite/silicon tandem solar cells; 2) PSCs; 3) silicon thin-film solar cells; 4) light management materials, including transparent conductive oxides, up-conversion materials, 5) solar to hydrogen conversion, and so on.